MAGNETIC NANOPARTICLES FOR ENHANCED OIL RECOVERY (EOR) USING EM METHODS

FATIHAH BINTI MOHAMAD AZMAN

ELECTRICAL & ELECTRONICS ENGINEERING
UNIVERSITI TEKNOLOGI PETRONAS
JUNE 2010

MAGNETIC NANOPARTICLES FOR ENHANCED OIL RECOVERY (EOR) USING EM METHODS

By

FATHEHAH BT MOHAMAD AZMAN

FINAL PROJECT REPORT

Submitted to the Electrical & Electronics Engineering Programme
in Partial Fulfillment of the Requirements
for the Degree
Bachelor of Engineering (Hons)
(Electrical & Electronics Engineering)

Universiti Teknologi PETRONAS
Bandar Seri Iskandar
31750 Tronoh
Perak Darul Ridzuan

CERTIFICATION OF APPROVAL

MAGNETIC NANOPARTICLES FOR ENHANCED OIL RECOVERY (EOR) USING EM METHODS

by

Fathehah Bt Mohamad Azman

A project dissertation submitted to the
Electrical & Electronics Engineering Programme
Universiti Teknologi PETRONAS
in partial fulfilment of the requirement for the
Bachelor of Engineering (Hons)
(Electrical & Electronics Engineering)

Approved:

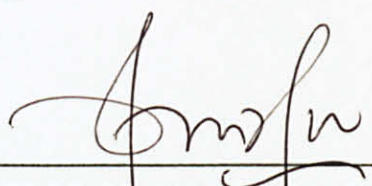

ASSOC. PROF. DR. NOORHANA YAHYA
Project Supervisor

DR NOORHANA YAHYA
Associate Professor
Fundamental & Applied Sciences Department
Universiti Teknologi PETRONAS, PERAK

UNIVERSITI TEKNOLOGI PETRONAS

TRONOH, PERAK

June 2010

CERTIFICATION OF ORIGINALITY

This is to certify that I am responsible for the work submitted in this project, that the original work is my own except as specified in the references and acknowledgements, and that the original work contained herein have not been undertaken or done by unspecified sources or persons.

FATHEHAH BT MOHAMAD AZMAN

CERTIFICATION OF ORIGINALITY

This is to certify that I am responsible for the work submitted in this project, that the original work is my own except as specified in the references and acknowledgements, and that the original work contained herein have not been undertaken or done by unspecified sources or persons.

FATHEHAH BT MOHAMAD AZMAN

ABSTRACT

Nickel nitrate, zinc nitrate and iron nitrate were used to synthesize nanosize nickel zinc ferrite ($Ni_{0.8}Zn_{0.2}Fe_2O_4$). The synthesis of nickel zinc ferrite has been extensively investigated in recent years because of their favorable properties such as high resistivity, low eddy current losses and high saturation magnetization [1]. Therefore, it plays an important role in many technological applications, such as high density magnetic recording media and electromagnetic wave absorption materials [2]. This project deals with synthesis of nickel zinc ferrite nanoparticle using sol-gel methods. Stoichiometric mixture of nickel (II) nitrate, Ni $(NO_3)_26H_2O$; zinc (II) nitrate, Zn $(NO_3)_26H_2O$; and iron (III) nitrate, Fe $(NO_3)_39H_2O$; were dissolved in aqueous solutions of 150 ml nitric acid HNO_3. The mixtures were annealed at 700°C, 900°C and 1200°C. Characterizations were done by using X-Ray Diffractions (XRD), Field Emission Scanning Electron Microscope (FESEM) and Energy Dispersion X-ray Spectroscopy (EDX). From analysis, it shows that by using XRD characterization, the highest peak intensity is observed for [3 1 1] plane at 2-theta. The particle sizes are in the range of 35.06 nm to 106.99 nm calculated using Scherer's equation. FESEM results show the grain size of nanoparticle which is in range of 50nm-150nm. It was found that grain size increases as the sintering temperature increased from 700 °C to 1200°C. The ferrite powder was also characterized for permeability, relative loss factor and Q-factor. The initial permeability was found to increase and relative loss factor decreased at high frequency. $Ni_{0.8}Zn_{0.2}Fe_2O_4$ nanoparticles prepared at low temperature exhibit good crystal structure, fine grain size and good magnetic properties. The synthesis nanoparticles were then injected into core sample for oil recovery purposes. After conducting experiment at low frequency (1KHz), results shows that by using nanoparticle, about 23.7% OOIP of oil can be recover compared to only 12.7% OOIP without using nanoparticle.

ACKNOWLEDGEMENT

I would like to express my gratitude to all those who help me to complete this final year research project. First of all, I want to thank to Electrical and Electronics Engineering Department, Chemical Engineering Department, Mechanical Engineering Department, and Geosciences and Petroleum Engineering Department for giving me permission to do the necessary research work and to use the facilities under their department.

I am deeply indebted to my supervisor Associate Professor Dr. Noorhana Binti Yahya for her help and support to complete this project. I have furthermore to thank the postgraduate students and my colleagues for their stimulating support, assistance and encouragement to go ahead with my thesis especially to Khaled Abdalla Elraies, Poppy Puspitasari and Nurul Shahida Salleh. I want to thank them for all their help, support, interest and valuable hints.

Last but not least, I would like to give my special thanks to all my family members especially my beloved mother and father, also my brother and sister for their motivation and emotion support to enabled me to complete this work. The preparation of this document would not have been possible without the support, hard work and endless efforts of a large number of individuals and institutions.

Thank you!

TABLE OF CONTENTS

LIST OF FIGURES

LIST OF TABLE

CHAPTER 1

INTRODUCTION

1.1 Background of Study

Advanced technology is trying to explore ways to enhance the nation's energy resources. There are several challenges for deepwater field developments in order to meet the demand of oil and gas exploration. The current state of the art of technology for the oil and gas exploration is EOR.

Enhanced oil recovery (EOR) is a technique for increasing the amount of crude oil that can be extracted from an oil field. Traditionally, chemical substance like carbon dioxide (CO_2) and polymer are used for EOR. Other than that, EOR also used methods like steam injection and gas injection. [3] Nowadays, physicist and electrical engineers are trying to prove that electromagnetic waves could be also applied to be used as one of the EOR methods. The purpose of EOR is to increase oil production, primarily through an increase in temperature, pressure, or an enhancement of the oil's ability to flow (low viscosity) through the reservoir. Research showing that by using EOR, we can improve about 30% to 60% of the reservoir's original oil compared with 20% to 40% using the primary and secondary recovery. [3]

EM waves can be used in deep water because of its ability to propagate into the sub-sea surface to detect the presence of hydrocarbon reservoir. Therefore, EM waves got the potential to be used inside the reservoir. The main concept is to transmit, to detect and to dissipate heat to the environment. This new methods hope to open new frontier in oil and gas exploration.

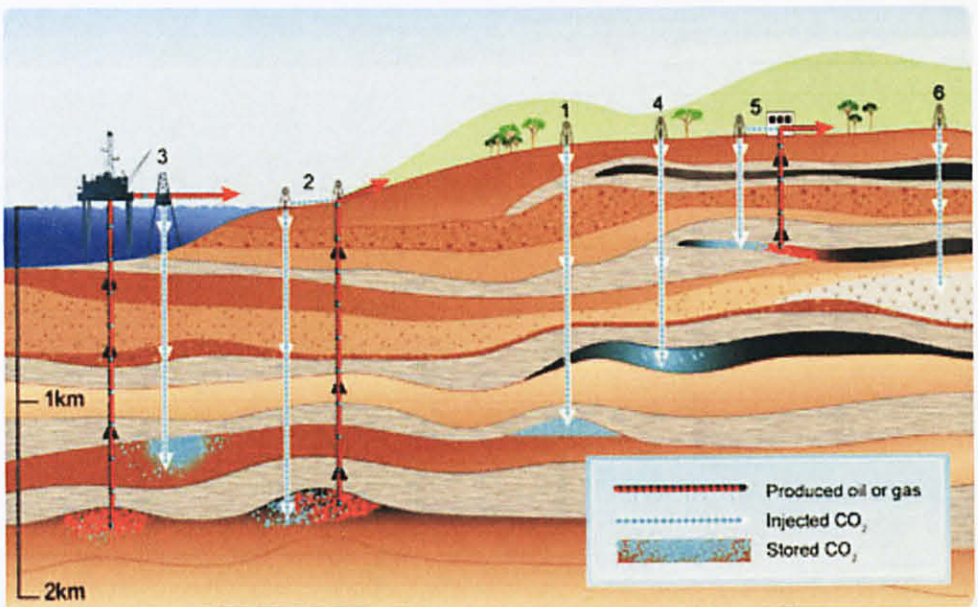

Figure 1: CO2 injection for EOR [4]

1.2 Problem Statement

To recover the left oil from reservoir is still remains as a challenge to the industry.

.

1.3 Objective and Scope of Study

1.3.1 Objectives

- To synthesis nickel zinc ferrite $Ni_{0.8}Zn_{0.2}Fe_2O_4$ nanoparticles by using sol-gel method.
- To characterize the nickel zinc ferrite nanoparticles by using X-Ray Diffractions (XRD), Field Emission Scanning Electron Microscope (FESEM), Energy Dispersion X-ray Spectroscopy (EDX) and also magnetic properties.
- To test the ability of magnetic nanoparticle to improve the oil recovery.

1.3.2 Scope of study

The area of study for this project will be divided to 2 parts: first part is synthesis and characterize the nanoparticle detector. Second part is the experiment of oil recovery which consists of transmitter, fluxgate magnetometer, core rock sample as well as the environment to be applied. The target user is for the petroleum industry .Thus, the scope of study covers for:

- The material and method to develop the nano sized detector.
- To carry out some research and experimental work to the real environment to be deal with.
- To calculate the oil recovery for core sample.

CHAPTER 2

LITERATURE REVIEW

2.1. Magnetic Nanoparticle

Magnetic nanoparticles are nanoparticle which can be manipulated using magnetic field. Examples of commonly particles that consist of magnetic elements are iron, nickel and cobalt. The physical and chemical properties of magnetic nanoparticles largely depend on the synthesis method and chemical structure. In most cases, the particles range from 1 to 100 nm in size.

Nanoparticles are of great scientific interest as they are effectively a bridge between bulk materials and atomic or molecular structures. A bulk ferrite should have constant physical and magnetic properties regardless of its size, but for nano-scale materials this is not often the case and their properties will change as their size approaches to nanoscale. This is due to the fact that the percentage of atoms at the surface become significant in comparison to volume ones. Nanoparticles exhibit a number special property relative to bulk material [5]. For this reason, there are new techniques to produce particles of different nanosizes with a good grade of homogeneity. Several techniques have been used for the preparation of pure Ni-Zn ferrite and substituted Ni-Zn ferrite nanoparticles. These include coprecipitation, hydrothermal, sol gel, high energy milling, etc. Solution methods, particularly the sol

Gel and self-combustion, have overcome the problem of improving or increasing the performance of the substituted Ni-Zn ferrite nanoparticles [6]

Nowadays, science and engineering has shown a rapid increase in interest for materials at the nano-scale. Nano-materials have attracted such a strong interest because of the physical, electronic, and magnetic properties resulting from their quantum size. Magnetic nano-particle applications are being investigated in multiple disciplines from biomedical sensors, drug delivery, magnetic resonance imaging, data storage, nano-electronics, etc.

Figure 2: Example of magnetic nanoparticle [7]

2.2 Electromagnetic detector

A detector or sensor is a device that measure physical quantity and converts it into signal which can be read by an observer or by instrument. Electromagnetic detector therefore is a device that measure electromagnetic waves that have been detected and convert it into signal which can be read in graphical or numerical by observer.

The electromagnetic receivers must be capable of measuring field strength that vary greatly in magnitude, from weak signals to strong direct signals from the source. Besides, it also should be capable to measuring the EM phase with respect to the source requires precise measurement of the timing of the signal.

2.3 Sol gel technique for preparation of nickel zinc ferrite

The sol-gel method is a useful and attractive technique for the preparation of nanosized particles because of its advantages which is good stoichiometric and the production of ultrafine particles with a narrow size distribution in a relatively short processing time at lower temperatures. [8]

Nickel zinc ferrite ($Ni_{0.8}Zn_{0.2}Fe_2O_4$) is a well known spinel magnetic material. Among the various existing methods of chemical synthesis, sol gel method is an alternative and promising technique for preparing soft ferrites, leading to highly pure, chemically homogeneous, and nanometric scale particles. [9]

According to Stefen Goerlich of Jenoptik L.O.S in Jena, traditional waveguide technologies such as ion exchange in glasses and titanium diffusion in litium niobate are relatively costly especially when production quantities are small. The sol gel process he said has the potential to produce less expensive elements

containing fiber alignment structures. The benefit of this method are the product quality can be controlled by ensuring the purity of the basic materials and the optical properties can be tailored easily by doping the basic materials or adding colloidal particle.

2.4 Electromagnetic waves for EOR

The using of electromagnetic heating on recovery of heavy oil reservoirs containing a bottom-water zone have be done by researcher from Alaska. They reported that electromagnetic heating is practically limited to small radius but becomes effective in combination with horizontal wells. It was further reported that the recovery can be enhanced by coupling the electromagnetic heating with gas or water injection in order to create the favorable pressure gradient in the presence of bottom water. The model showed that a recovery as high as 77% of oil in place (OIP) was obtained. [10]

Chakma and Jha (1992) conducted the study which showed that the heat losses in the reservoir in case of electromagnetic heating can be kept to a minimum by confining the heating to the oil-bearing zone only. Water saturation, salinity of brine, and frequency of electromagnetic waves are the major factors affecting the heat transfer in the reservoir. The presence of water is essential for continuous propagation of waves. The study reported the yield of 45% of oil initially in place of heavy oil of moderate viscosity was recovered. [11]

Another study reported that the effects of temperature rise due to microwave heating on various concentrations of crude oil under different exposure times (Bjorndalen et al., 2005). The study concluded that, with an increase in density of the fluid, there is a decrease in the temperature change with time. [12]

2.5Theory

2.5.1 Electromagnetic wave

Electromagnetic waves can be imagined as a self-propagating transverse oscillating wave of electric and magnetic fields. This diagram shows a plane linearly polarized wave propagating from right to left. The electric field is in a vertical plane, the magnetic field in a horizontal plane.

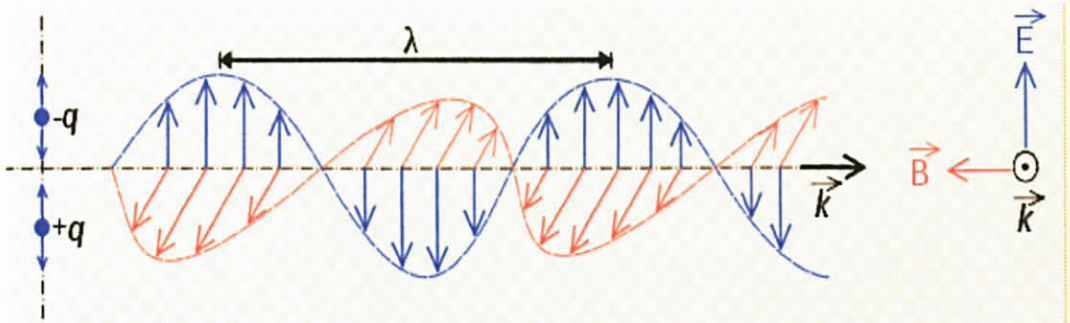

Figure 3: Electromagnetic propagation [13]

Where;

λ= wavelength

$\vec{E}$ = electric field

$\vec{B}$ = magnetic field

2.5.2 Lenz law

When a magnet is moved past a conductive material, two things will happen. First, the moving magnetic field cuts through the conductor and induces eddy currents in the conductor. This is discovered by the English scientist, Michael Faraday. Next, the eddy currents in the conductor generate their own magnetic field, (secondary magnetic field) which opposes the original or primary magnetic field. This directional relationship between the induced magnetic fields and current is known as Lenz's Law. Picture below shows show the induction of eddy currents and Lenz's Law.

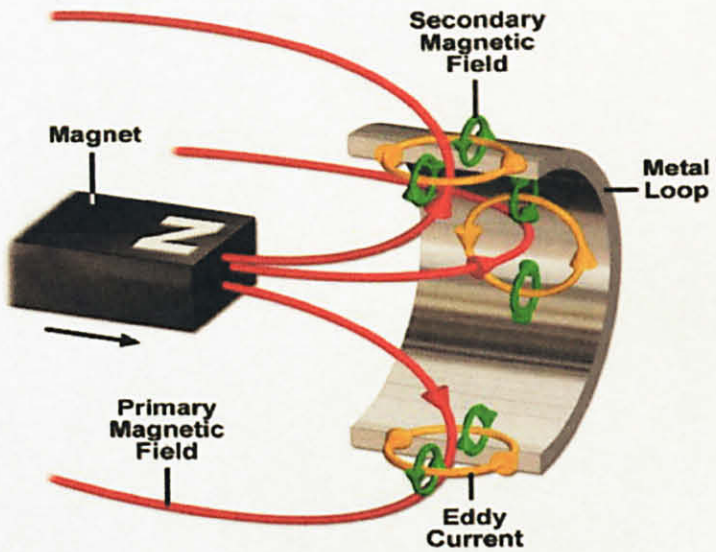

Figure 4: Induction of eddy current and magnetic field [14]

Heat is produced by two ways which are first through the eddy current and second through the hysteresis. For eddy current, heat generated is actually comes from current carrying conductor or the heating element. While for hysteresis, the losses are due to the magnetic material. Magnetic materials here are referred to the ferromagnetic or 'ferromagnetism' phenomenon. Ferromagnetism is the ability of a

material to spontaneously become a permanent magnet whenever an external magnetic field is applied to it. The hysteresis losses in the material used is due to the relative permeability of the material itself.

Magnetic permeability μ, are the ability of the material to magnetize in response to the magnetic field. The relation of permeability in electromagnetism can be describe as: [15]

$$B = \mu_0 . H$$

Where,

B= magnetic flux density within the material

μ_0= The material relative permeability

H= Applied magnetic field

CHAPTER 3

METHODOLOGY

3.1 Project Identification

3.1.1 Project flow

Basically, this project is divided into four stages which are:

1. Research on the background of the project
2. Synthesis nickel zinc ferrite nanoparticle via sol-gel method.
3. Characterization nickel zinc ferrite nanoparticle
4. Experiment of oil recovery using EM methods

This project begins with the research on current methods used for enhance oil recovery (EOR). Research has been done to get an overview on latest technology that can improve the efficiency of EOR. Research also been made on electromagnetic technology. Such case study is needed to understand the problem encounter and find out the best solution for it.

Next stage is the design stage. At this phase, the main focus is more on material selection. The aim of the project is to develop nanoparticles that can be the medium to absorb EM waves and assist the oil recovery at the same time. The heat release should be sufficient enough to help the crude oil to have a better flow.

Therefore, selection of the material for the nanoparticle detector should satisfy the criteria

Third stage is synthesis and characterization of nickel zinc ferrite nanoparticle. Nanoparticles of nickel zinc ferrite were prepared by sol-gel method. After that, characterizations were done by using X-Ray Diffractions (XRD), Field Emission Scanning Electron Microscope (FESEM), Energy Dispersion X-ray Spectroscopy (EDX) and also magnetic characterization to get data for permeability, relative loss factor and Q-factor.

Next, project will be continuing by Experiment of oil recovery using EM methods. Two core samples will be used for the experiment. One is flooded with brine water and crude oil while the other core is flooded with brine water, crude oil and also nanoparticles. Finally, the percentage of oil recovery will be calculated. Experimental works were done which is something similar to the real environment to be deal with.

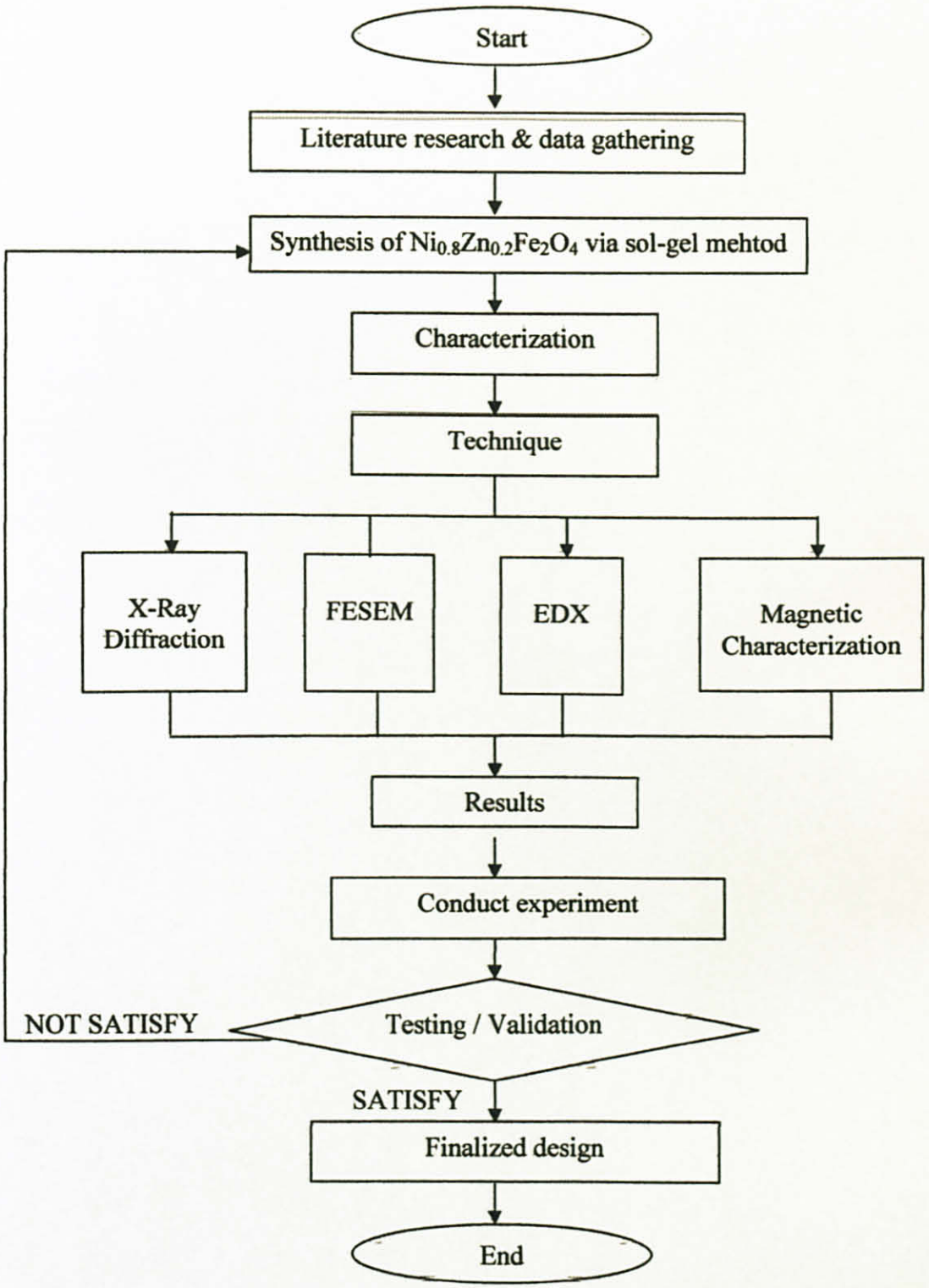

Figure 5: Project Process Flow Chart

3.2 Tools Required

Software and hardware are needed upon completion of this project. The tools required are listed as below:

3.2.1 X-Ray Diffraction (XRD)

X-ray scattering techniques are a family of non-destructive analytical techniques which reveal information about the crystallographic structure, chemical composition, and physical properties of materials and thin films. These techniques are based on observing the scattered intensity of an X-ray beam hitting a sample as a function of incident and scattered angle, polarization, and wavelength or energy. [16]

X-ray diffraction finds the geometry or shape of a molecule using X-rays. X-ray diffraction techniques are based on the elastic scattering of X-rays from structures that have long range order. The most comprehensive description of scattering from crystals is given by the dynamical theory of diffraction.[16]

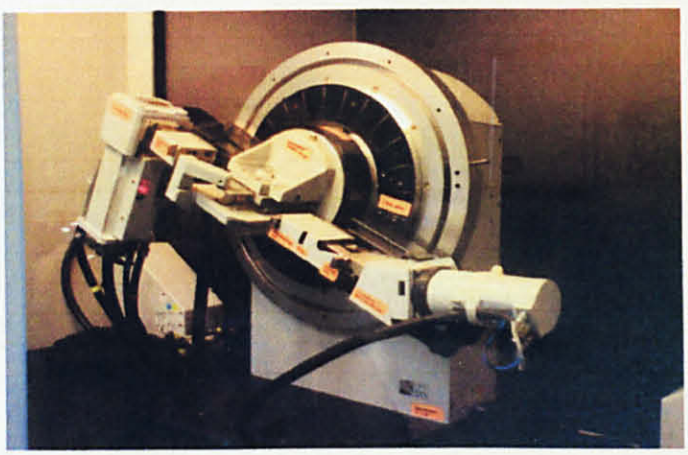

Figure 6: X-Ray Diffraction Machine

3.2.2 Field Emission Scanning Electron Microscope (FESEM)

A field-emission cathode in the electron gun of a scanning electron microscope provides narrower probing beams at low as well as high electron energy, resulting in both improved spatial resolution and minimized sample charging and damage. The application of FESEM include Semiconductor device cross section analyses for gate widths, gate oxides, film thicknesses, and construction details, advanced coating thickness and structure uniformity determination and small contamination feature geometry and elemental composition measurement. FESEM is needed because of;

i. FESEM produces clearer, less electrostatically distorted images with spatial resolution down to 1 1/2 nm. That's 3 to 6 times better than conventional SEM.

ii. Smaller-area contamination spots can be examined at electron accelerating voltages compatible with Energy Dispersive X-ray Spectroscopy.

iii. Reduced penetration of low kinetic energy electrons probes closer tothe immediate material surface.

iv. High quality, low voltage images are obtained with negligible electrical charging of samples. (Accelerating voltages range from 0.5 to 30 kV.)

v. Need for placing conducting coatings on insulating materials is virtually eliminated.[17]

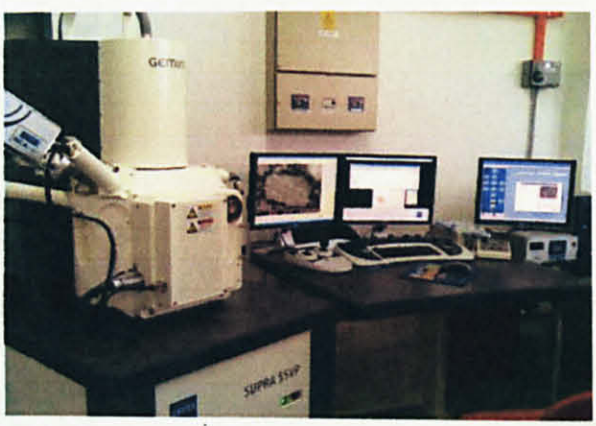

Figure 7: Field Emission Scanning Electron Microscope

3.2.3 Energy Dispersive X-ray spectroscopy (EDX)

Energy dispersive X-ray spectroscopy (EDX) is an analytical technique used for the elemental analysis or chemical characterization of a sample. It is one of the variants of XRF. As a type of spectroscopy, it relies on the investigation of a sample through interactions between electromagnetic radiation and matter, analyzing x-rays emitted by the matter in response to being hit with charged particles. Its characterization capabilities are due in large part to the fundamental principle that each element has a unique atomic structure allowing x-rays that are characteristic of an element's atomic structure to be identified uniquely from each other [18].

3.2.4 LCR vector network analyzer

LCR vector network analyzer is used to get the data for the initial permeability and Q-factor for the respective toroids.

Figure 8: LCR vector network analyzer

3.2.5 Hardware required

- Transmitter

. Transmitter is used to transmit the electromagnetic waves. This transmitter is a hexagon shape with 15 cm length for every segment. It was constructed with six segments from 6m of copper wire winding and with 6 sources.

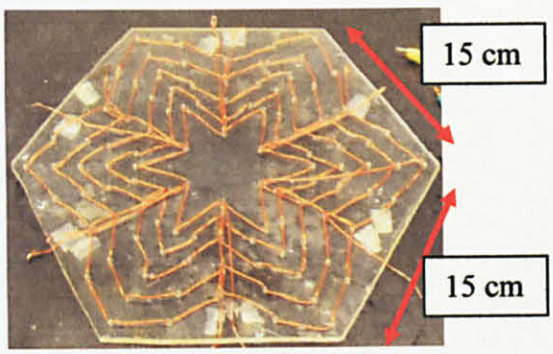

Figure 9: Hexagon shape transmitter

- Amplifier

Power amplifier was used to amplify the signal. So, more EM waves can be transmitted. This amplifier is operated by supplying 12V DC supply and 1 KHz frequency

Figure 10: Amplifier

- Nanoparticle magnetic feeder

Magnetic Feeder was used to increase amplitude of EM waves transmitted by the designed transmitter. Nickel zinc ferrite magnetic feeder was prepared via sol gel method.

Figure 11: Nanoparticle magnetic feeder

- Tank

A tank with full of brine water with density 1.0061g/cm^3 is used to place all the equipment for the experiment. The tank size dimension is 1.92m X 0.91m X 0.61m

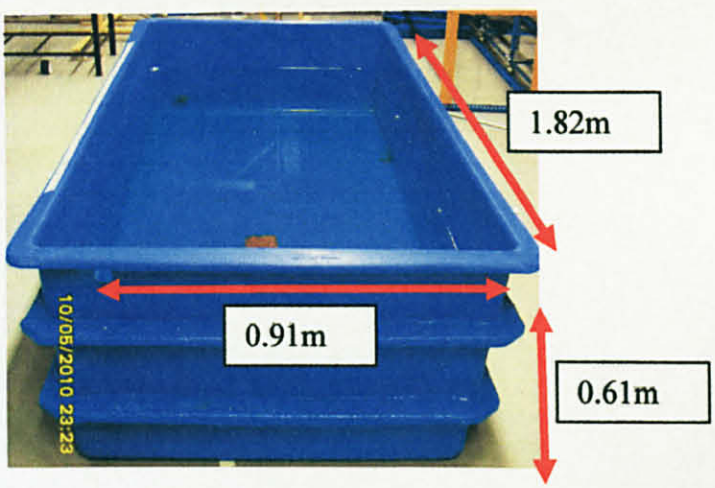

Figure 12: Tank

- Decaport data acquisition system (DAS) Model NI PXI-1042 and Fluxgate Magnetometer

Fluxgate Magnetometer was used in order to detect EM waves and DAS is used to store the data of the transmitted EM waves.

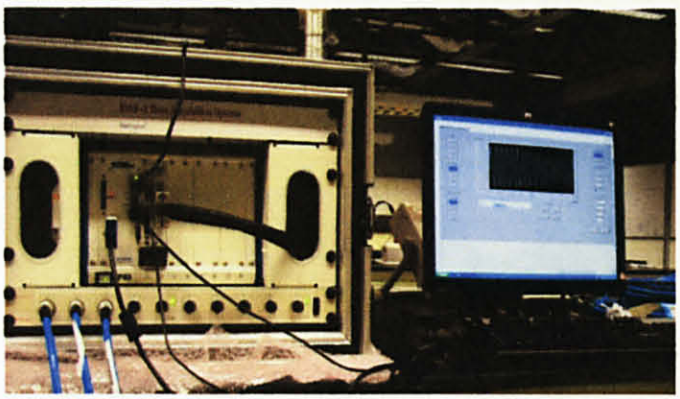

Figure 13: Data acquisition system (DAS)

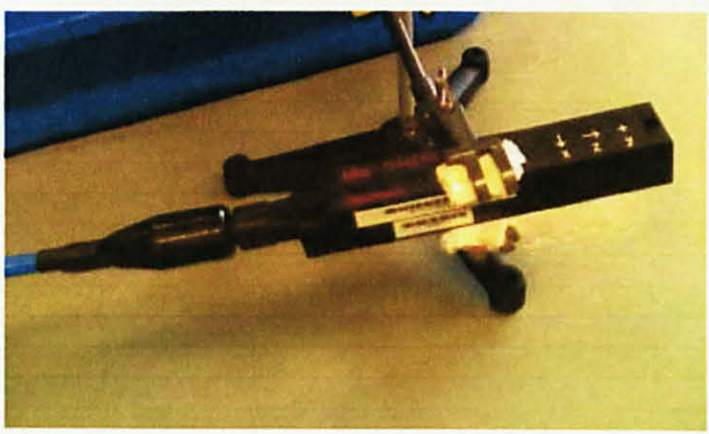

Figure 14: Fluxgate magnetometer

- Function generator

Function generator was used to supply 1 KHz frequency to transmitter and magnetic feeder.

Figure 15: Function generator 5MHz model Instek GFG-8250A

- DC Power Supply

Dc power supply was used to supply the amplifier with 12V.

Figure 16: DC Power Supply

- Temperature controller

The temperature controller Protech SDC10 was used to increased and maintains the temperature of brine water inside the tank about 36°C-37°C.

Figure 17: Protech SDC10 Temperature controller

- Balance

Balance was used to weigh the materials and core sample. It gives accurate reading up to 4 decimal points.

Figure 18: Balance

- Helium porosimeter

Helium pososimeter was used in order to characterize the core samples to get the pore volume, porosity and permeability data. Porosity is the percentage that the volume of the pore space bears to the total bulk volume, which is the pore space that determines the amount of space available for storage of fluids. Pore volume is the volume of connected pores in a core sample in which the fluids can flow, and permeability is the ability of a rock to transmit fluid through the pore spaces

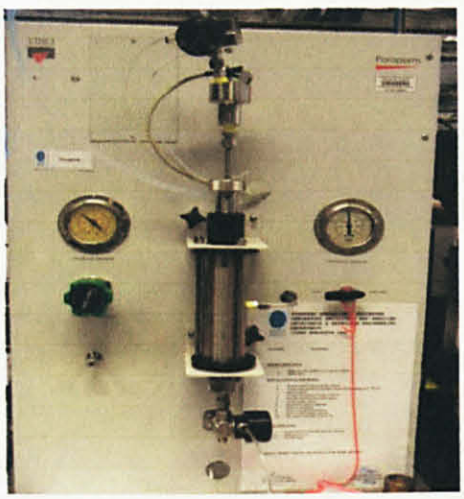

Figure 19: Helium porosimeter

- Core flooding machine

Core flooding machine was used in order to prepare the core sample with the brine, crude oil and also with the nanoparticles. The process of the flooding was involved with the used of injection of brine and crude oil at a high pressure and low flow rates.

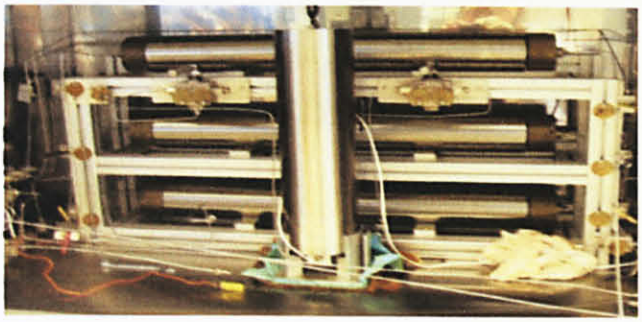

Figure 20: Core flooding machine

- Core sample

Table 1: Core rock sample properties

Core rock sample	A1 	A2 
Permeability (mD)	567.800	532.435
Pore Volume V_p (cc)	17.766	18.297
Porosity Φ(%)	21.177	20.715
V_{grain} (g/cc)	66.125	70.028
V_{bulk} (g/cc)	83.891	88.324
Weight (g)	173.535	180.199
Diameter (mm)	38.080	38.120
Length (mm)	73.660	77.390

CHAPTER 4

RESULTS AND DISCUSSIONS

4.1 Synthesis of Nickel Zinc Ferrite

4.1.1 Experimental Procedure

Metal nitrates such as nickel nitrate [(Ni $(NO_3)_2.6H_2O$)], zinc nitrate [(Zn $(NO_3)_2.6H_2O$)], iron nitrate [(Fe $(NO_3)_3.9H_2O$)], and nitric acid (HNO_3), were used as raw materials. All metal nitrates used in the fabrication of $Ni_{0.8}Zn_{0.2}Fe_2O_4$ were dissolved in the aqueous solution of 150 ml nitric acid HNO_3. Following calculations is done in order to prepare 20g of $Ni_{0.8}Zn_{0.2}Fe_2O_4$ by using sol gel technique. Details of the calculations are simplified in table 1.

4.1.2 Calculation of nickel zinc ferrite ($Ni_{0.8}Zn_{0.2}Fe_2O_4$) using sol-gel method

Starting materials are Nickel nitrate, Ni $(NO_3)_2.6H_2O$, Zinc nitrate, Zn $(NO_3)_2.6H_2O$ and Iron nitrate, Fe $(NO_3)_3.9H_2O$

Figure 21: Material used

- Balance equation:

$0.8\ Ni(NO_3)_2.6H_2O + 0.2\ Zn(NO_3)_2.6H_2O + 2Fe(NO_3)_3.9H_2O \rightarrow Ni_{0.8}Zn_{0.2}Fe_2O_4$

Relative molecular mass for nickel nitrate

I. $Ni(NO_3)_2.6H_2O$ (considering H_2O)

$= (58.693) + (2 \times 14.007) + (6 \times 15.999) + (12 \times 1.0079) + (6 \times 15.994)$

$= 58.693 + 28.014 + 95.994 + 12.0948 + 95.964$

$= 290.7598$ g/mol

II. $Ni(NO_3)_2$ (without considering H_2O)

$= 290.7598 - (12.0948 + 95.964)$

$= 182.701$ g/mol

Relative molecular mass for zinc nitrate

I. $Zn(NO_3)_2.6H_2O$ (considering H_2O)

$= (65.4090) + (2x14.0067) + (12x15.9994) + (12x1.00794)$

$= 297.427$ g/mol

II. $Zn(NO_3)_2$ (without considering H_2O)

$= 297.427 - (12.0948 + 95.964)$

$= 189.3682$ g/mol

Relative molecular mass for iron nitrate

I. $Fe(NO_3)_3.9H_2O$ (considering water)

$= (55.845) + (3 \times 14.007) + (9 \times 15.999) + (18 \times 1.0079) + (9 \times 15.994)$

$= 55.845 + 42.021 + 143.991 + 18.1422 + 143.946$

$= 403.9542$ g/mol

II. $2Fe(NO_3)_3$ (without water)

$= 403.9542 - (18.1422 + 143.946)$

$= 241.8604$ g/mol

- To prepare 20g of $Ni_{0.8}Zn_{0.2}Fe_2O_4$

Mass of salt needed without water

$$Ni\ (NO_3)_2 = \frac{146.1626}{667.7671} \times 20g = 4.3777g$$

$$Zn\ (NO_3)_2 = \frac{37.8838}{667.7671} \times 20g = 1.1346g$$

$$Fe\ (NO_3)_3 = \frac{483.732}{667.7671} \times 20g = 14.4877g$$

Mass of hydrated salt needed with water

$$Ni\ (NO_3)_2.6H_2O = \frac{232.6359}{146.1626} \times 4.3777g = 6.968g$$

$$Zn\ (NO_3)_2.6H_2O = \frac{37.8838}{667.7671} \times 20g = 1.7816g$$

$$Fe\ (NO_3)_3.9H_2O = \frac{807.9944}{483.7208} \times 14.4877g = 24.1998g$$

Table 2: Calculations for $Ni_{0.8}Zn_{0.2}Fe_2O_4$

Material	Without water	With water	20g without water	20g with water (final weight)
0.8 $Ni(NO_3)_2.6H_2O$	146.1626 $gmol^{-1}$	232.6359 $gmol^{-1}$	4.3777g	6.968g
0.2 $Zn(NO_3)_2.6H_2O$	37.8838 $gmol^{-1}$	59.4849 $gmol^{-1}$	1.1346g	1.7816g
2 $Fe(NO_3)_3.9H_2O$	483.7208 $gmol^{-1}$	807.9944 $gmol^{-1}$	14.4877g	24.1998g
TOTAL	667.7671 $gmol^{-1}$	1100.1153 $gmol^{-1}$	20g	32.9494g

The solutions were stirred at 250 r.p.m for 1 day separately and then were mix into one solution. Then, the mixture was stirred for another 1 day and then heated up gradually at 40°C, 50°C, 60°C and 70°C until gel-like solution was formed and the heating process is stopped immediately.

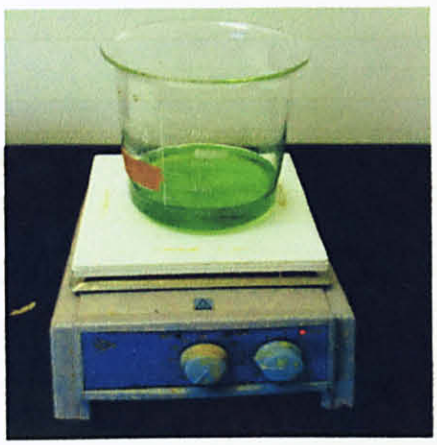

Figure 22: Stirring mixed solution for 24 hours

Figure 23: Gel formed

Then, the samples were dried in an oven at 110°C for 10 days for evaporation purpose. After that, the dried samples were crushed for 8 hours to obtain fine particles.

Figure 24: After drying

Figure 25: Crushing for 8 hours

Then, powder sintered at 700 °C,900°C and 1200 °C for 4 hours to get the required characteristics of ferrite powder.

Figure 26: Annealing

After annealing process is complete, the samples were crushed again for 2 hours. Then, these samples were characterized using X-Ray Diffractions (XRD), Field Emission Scanning Electron Microscope (FESEM) and Energy Dispersive X-Ray (EDX).

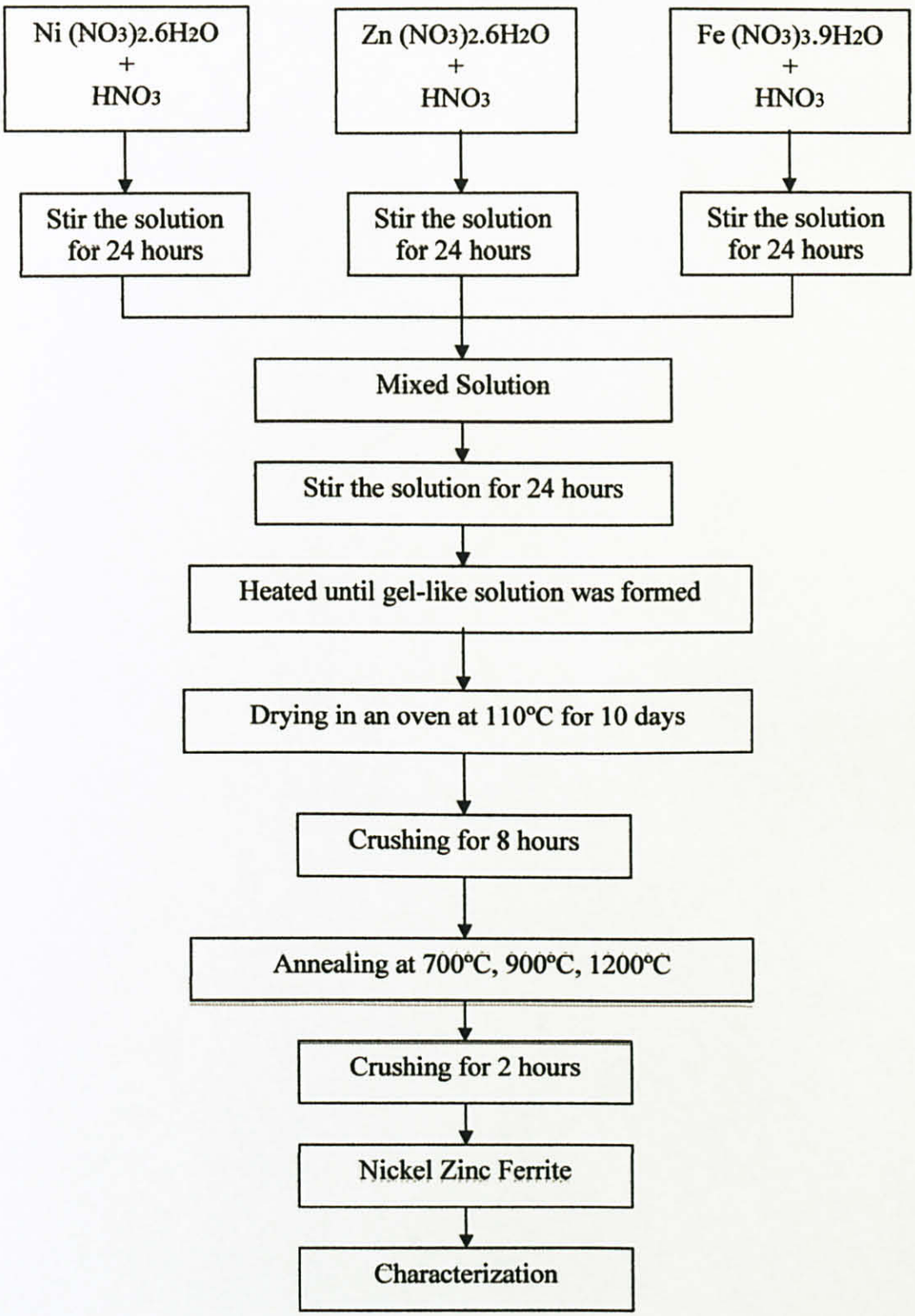

Figure 27: Flow chart of Sample prepared by sol-gel method

4.2 Characterization of Nickel Zinc Ferrite

4.2.1 X-Ray Diffraction (XRD) Results

The result gathered from the XRD is matched with the standard card of nickel zinc ferrite. Refer to Table 2.

Table 3: Standard Card of Nickel Zinc Ferrite

SAMPLE	STANDARD CARD
$Ni_{0.8}Zn_{0.2}Fe_2O_4$ (700^{O}C)	SS-NNNN 52-0277 (N)
$Ni_{0.8}Zn_{0.2}Fe_2O_4$ (900^{O}C)	SS-NNNN 52-0277 (N)
$Ni_{0.8}Zn_{0.2}Fe_2O_4$ (1200^{O}C)	SS-NNNN 52-0277 (N)

By applying Scherer equation the average crystallite size of the particles can be calculated. The Scherer's equation is: [19]

$$D = \frac{K\lambda}{\beta \cos\theta}$$

Where:

K = 0.9

λ = X-ray wavelength (1.5408 Åm)

β = FWHM 2θ

θ = Bragg's angle

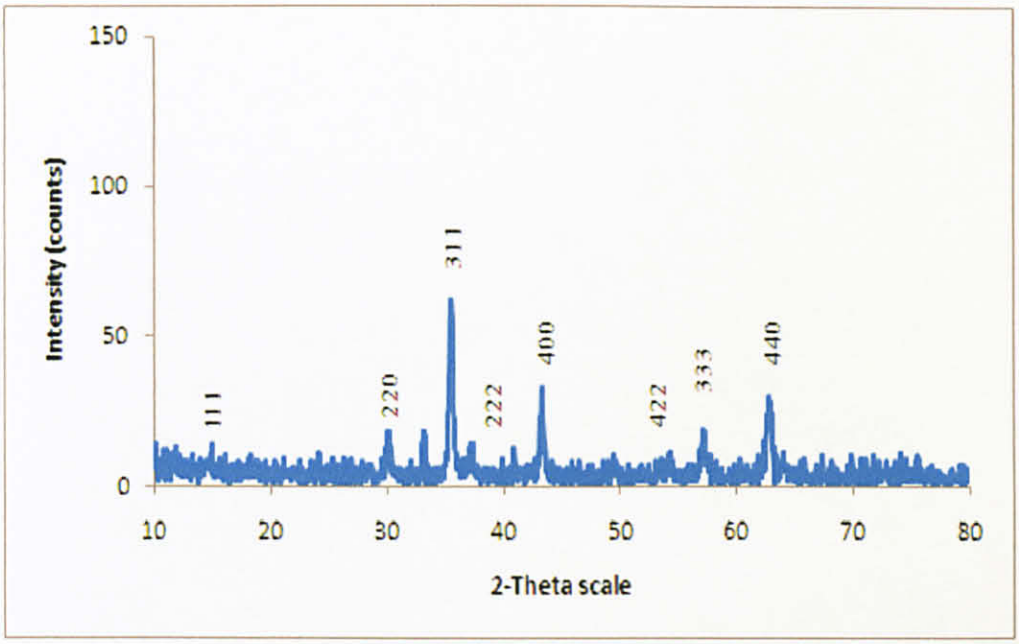

Figure 28: XRD result for $Ni_{0.8}Zn_{0.2}Fe_2O_4$ 700°C sample

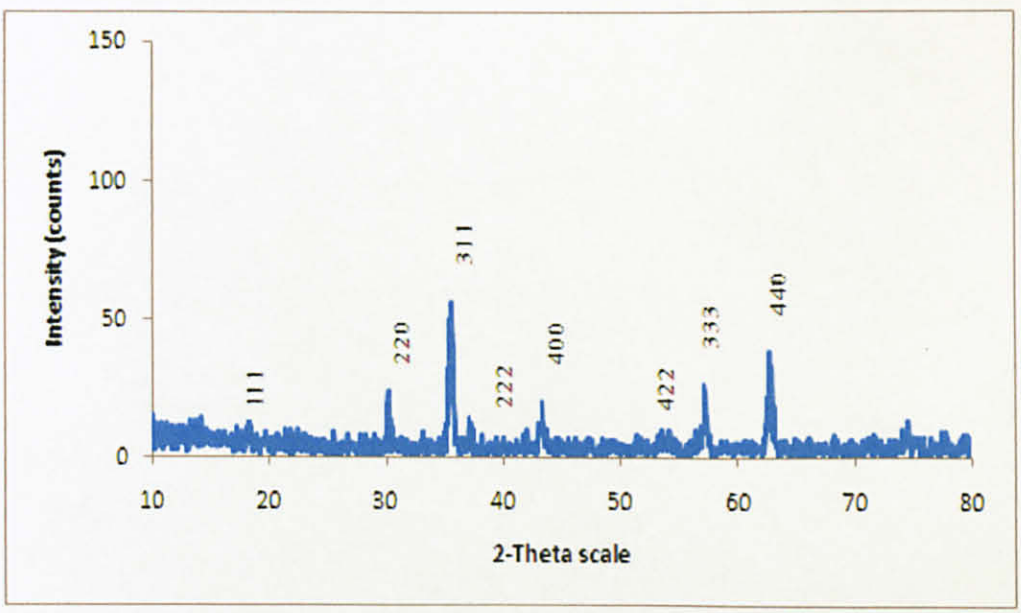

Figure 29: XRD result for $Ni_{0.8}Zn_{0.2}Fe_2O_4$ 900°C sample

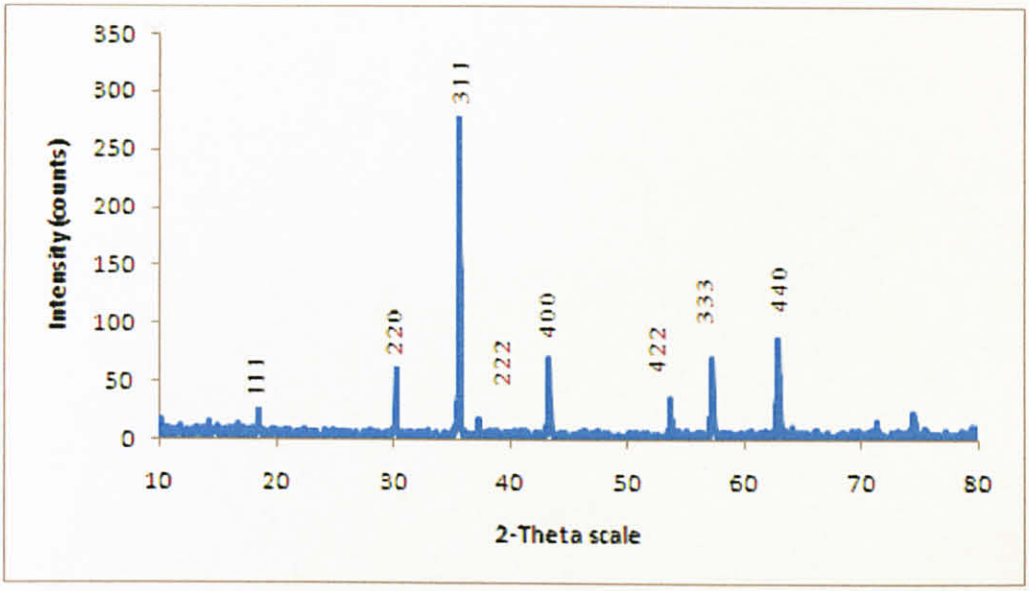

Figure 30: XRD result for $Ni_{0.8}Zn_{0.2}Fe_2O_4$ 1200°C sample

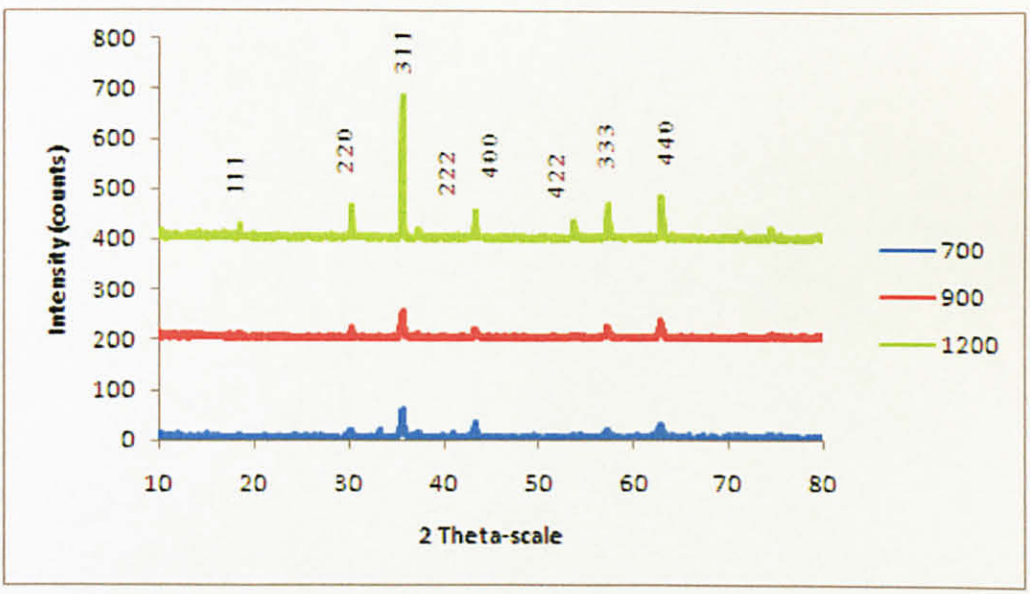

Figure 31: XRD patterns for $Ni_{0.8}Zn_{0.2}Fe_2O_4$ with [311] peak with annealed at temperatures 700 ˚C, 900 ˚C and 1200˚C.

Samples	X-Ray Diffraction (Correspond to [311] peaks)						
	Intensity (Counts)	FWHM	d-spacing (Å)	Crystallite size (nm)	a	b	c
700°C	56	0.238	2.52022	35.06	8.3696	8.3696	8.3696
900°C	62	0.238	2.52027	35.06	8.3696	8.3696	8.3696
1200°C	286	0.078	2.51972	106.99	8.3696	8.3696	8.3696

Table 4: XRD data for 3 samples with different annealing temperatures

Discussion

Table 3 shows the XRD analysis which identifies the value of full width half maxima (FWHM), d-spacing and crystallite size for the [311] plane as a high peak. Scherer's equation is used to determine the diameter of nickel zinc ferrite nanoparticle by using XRD results. From Table 3, it can be claimed that nickel zinc ferrite has cubic structure because alpha, beta and gamma are in 90 degree and the value of a, b, c are the same. From the table, it is cleared that as we increased the annealing temperature form 700 °C to 12000°C the crystallite size increases and also lattice parameter increases. However, we don't know the exact temperature when the lattice is formed since experiment is conducted for only three temperatures and not for every temperature. This is due to the time constraint and also expensive cost to conduct the experiment.

By applying Scherer equation 700°C sample and 900°C sample gives same crystallite size which is 35.06nm. However, 900°C is chosen because of higher intensity. The particle sizes are in the range of 35.06 nm to 106.99 nm calculated using Scherer's equation.

4.2.2 Field Emission Scanning Electron Microscope (FESEM) Results

Field Emission Scanning Electron Microscope (FESEM) is use to identify the morphology of nanostructure and dimension of grain size for bulk and nano-particle. Figure 17, 18, and 19 shows FESEM morphology for $Ni_{0.8}Zn_{0.2}Fe_2O_4$ annealed at 700˚C, 900˚C and 1200˚C.

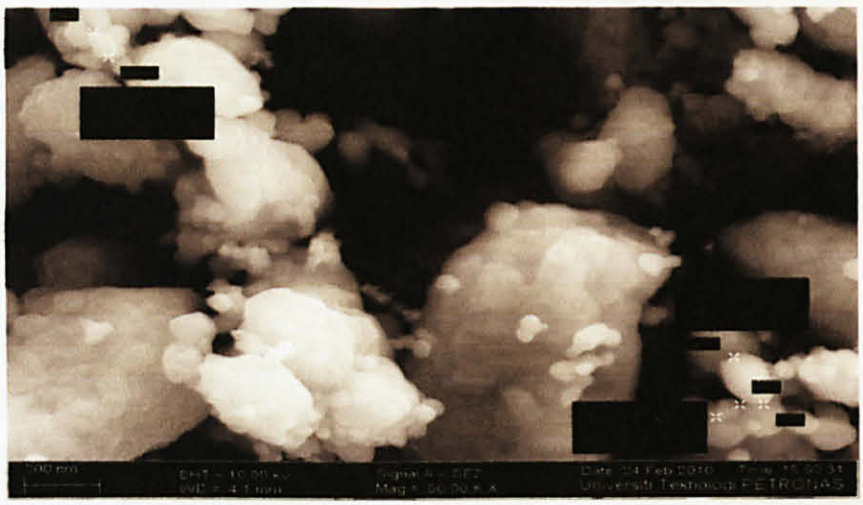

Figure 32: FESEM morphology for $Ni_{0.8}Zn_{0.2}Fe_2O_4$ annealed at 700˚C

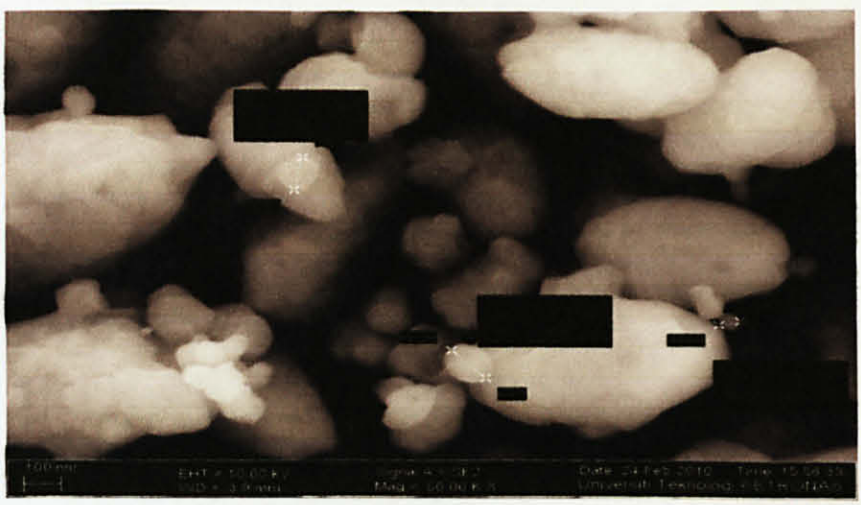

Figure 33: FESEM morphology for $Ni_{0.8}Zn_{0.2}Fe_2O_4$ annealed at 900˚C

Figure 34: FESEM morphology for $Ni_{0.8}Zn_{0.2}Fe_2O_4$ annealed at 1200˚C

Discussion:

For sample annealed at 700°C, the particle size in the range of 77nm to182nm. The second sample which annealed at 900 °C, the particle size in the range of 59nm to134nm. For the highest annealing temperature which is 1200°C, the particle size varies between 370nm to 429nm. However, the results are not accurate since the nanoparticles are agglomerated.

Results show that the grain size is increasing as the sintering temperature increases. For sample which annealed at 1200 ˚C for 4 hours, the morphology of $Ni_{0.8}Zn_{0.2}Fe_2O_4$ became more crystallite for nano-particles because annealing temperature causes more ions to move into the lattice crystal to be arranged as cubic arrangement. However, the particle size is very huge and not suitable to use for enhanced oil recovery.

4.2.3 Energy Dispersive X-Ray (EDX)

Energy Dispersive X-Ray (EDX) is a chemical microanalysis technique performed in conjunction with FESEM. Tables below shows that the atomic and weight percentage of the corresponding elements which are Nickel, Zinc, Ferum and Oxygen.

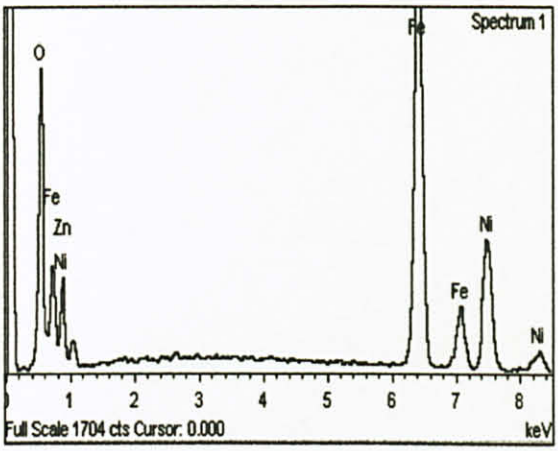

Element	Weight%	Atomic%
O K	21.49	49.52
Fe K	49.33	32.57
Ni K	22.71	14.26
Zn K	6.48	3.65
Totals	100.00	

Figure 35: Spectrum and EDX data for 700°C sample

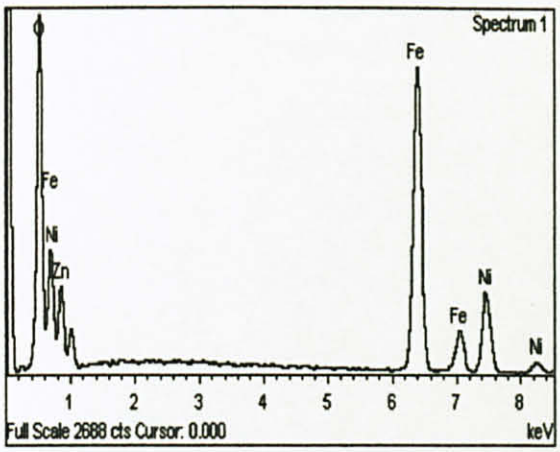

Element	Weight%	Atomic%
O K	31.28	61.99
Fe K	43.96	24.96
Ni K	18.97	10.24
Zn K	5.79	2.81
Totals	100.00	

Figure 36: Spectrum and EDX data for 900°C sample

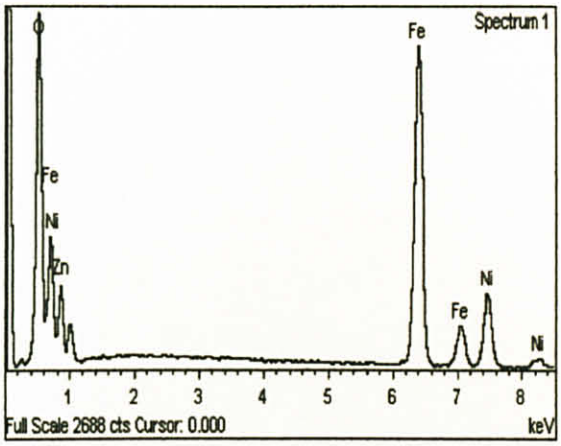

Element	Weight%	Atomic%
O K	30.90	61.57
Fe K	45.77	26.12
Ni K	16.96	9.21
Zn K	6.37	3.10
Totals	100.00	

Figure 37: Spectrum and EDX data for 1200°C sample

Theoretical value of atomic in percent (%) for $Ni_{0.8}Zn_{0.2}Fe_2O_4$ are calculated as below.

$Ni_{0.8}Zn_{0.2}Fe_2O_4 = 7$

$$Ni = \frac{0.8}{7} \times 100\% = 11.42\%$$

$$Zn = \frac{0.2}{7} \times 100\% = 2.85\%$$

$$Fe = \frac{2}{7} \times 100\% = 28.57\%$$

$$O = \frac{4}{7} \times 100\% = 57.14\%$$

Table 5: EDX data and standard deviation for $Ni_{0.8}Zn_{0.2}Fe_2O_4$ at 700°C, 800°C and 1200°C

Samples / Elements		700° C	900 °C	1200 °C
Ni	Weight (%)	22.71	18.97	16.96
	Atomic (%)	14.26	10.24	9.21
	Standard deviation (%)	24.87	10.33	19.35
Zn	Weight (%)	6.48	5.79	6.37
	Atomic (%)	3.65	2.81	3.10
	Standard deviation (%)	28.07	1.4	8.77
Fe	Weight (%)	49.33	43.96	45.77
	Atomic (%)	32.57	24.96	26.12
	Standard deviation (%)	14	12.64	8.58
O	Weight (%)	21.49	31.28	30.90
	Atomic (%)	49.52	61.99	61.45
	Standard deviation (%)	13.34	8.49	7.54

Discussions:

Experimental atomic value is compared with the theoretical atomic value. For element nickel and zinc, 900°C sample gives the lowest standard deviation value. However, for element ferum and oxygen, 1200°C sample gives the lowest standard deviation value compared to the other sample. 700°C sample give the highest standard deviation value for all elements.

4.2.4 Magnetic Characterization

The objective of doing the magnetic characterization is to analyse the initial permeability, Q-factor and relative loss factor for $Ni_{0.8}Zn_{0.2}Fe_2O_4$ nanoparticles.

$Ni_{0.8}Zn_{0.2}Fe_2O_4$ was fabricated in the form of toroid in order to perform the magnetic characterization. For the first step, 0.5g of the $Ni_{0.8}Zn_{0.2}Fe_2O_4$ powder was weighted. The weighted powder then was mixed with the polyvinyl alcohol (PVA) and crushed for several minutes. The powder was then moulded into toroid shape and was pressed with force of 3000 kg or 1500LB using autopallet pressing machine.

Figure 38: Autopallet press machine

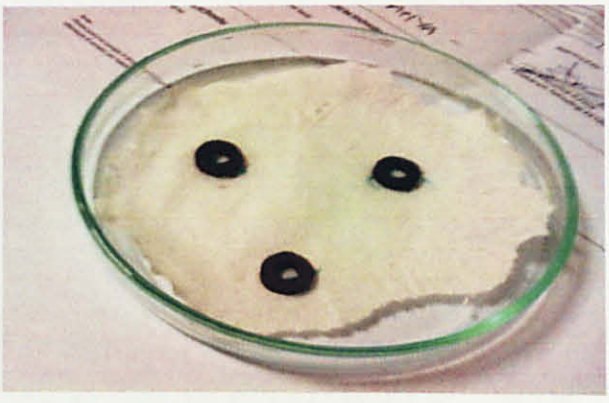

Figure 39: Toroids before sintering

Finally, the toroids were sintered at 1200C with 6 hours increments time, 4 hours holding time and 6 hours cooling time.

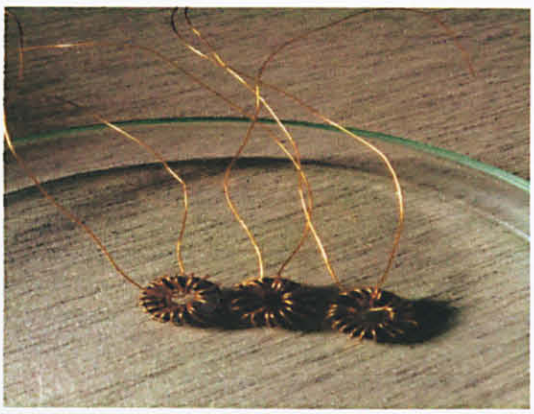

Figure 40: Toroids after sintered with 20 turns

Table 6: Properties for sample

Parameter	700° C	900° C	1200° C
Weight (g)	0.5	0.5	0.5
Outer Diameter (cm)	0.5	0.5	0.5
Inner Diameter (cm)	0.25	0.25	0.25
Height (cm)	0.25	0.25	0.25
Density (g/cm^3)	3.4	3.4	3.4
Quantity of toroid	1	1	1
Number of winding	20	20	20
Material of winding	Copper wire	Copper wire	Copper wire
Sintering time	1200 C	1200C	1200 C

LCR vector network analyzer is used to get the data for the initial permeability and Q-factor for the respective toroids.

Figure 41: LCR vector network analyzer

Initial permeability and relative loss factor (RLF) of $Ni_{0.8}Zn_{0.2}Fe_2O_4$ sintered at 700°C, 900°C and 1200°C were calculated by using LCR vector network analyzer by calculating the values of Ls and Q factor. The formula for Initial permeability μ_i is [20]

$$\mu_i = \frac{2\pi L_S}{N^2 \mu_o t \ln(Do/Di)}$$

Where:

L_s = is the series inductance,

μ_o = is the magnetic permeability,

D_o = is the outer diameter of the toroid,

D_i = is the inner diameter of the toroid, π

N = is the no of turns,

t = is the thickness of the toroid.

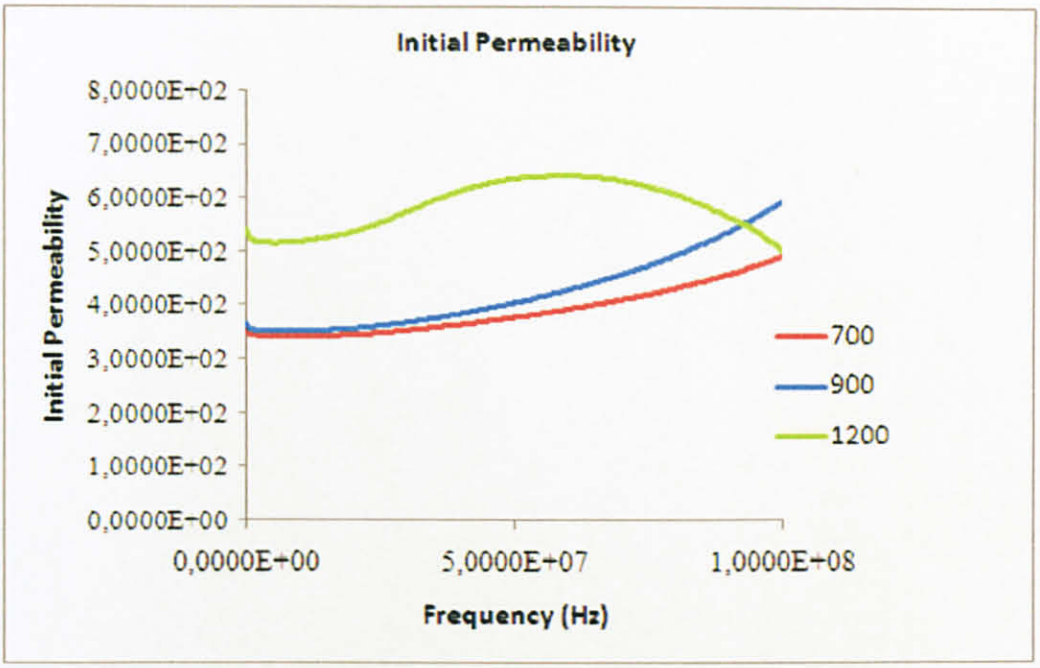

Figure 42: Initial permeability versus frequency for $Ni_{0.8}Zn_{0.2}Fe_2O_4$ toroid

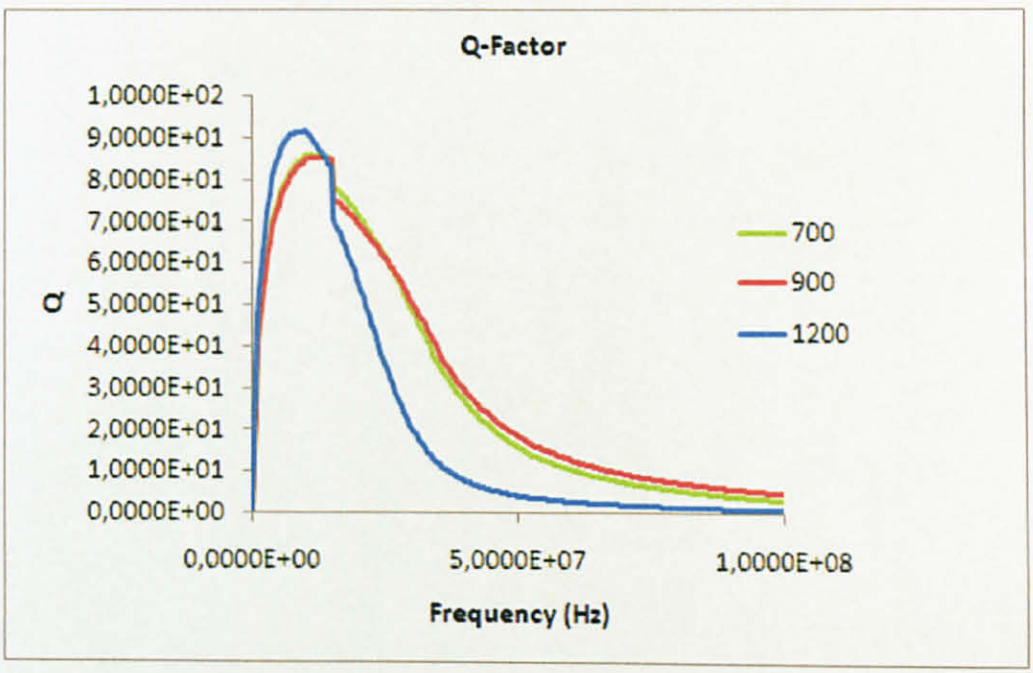

Figure 43: Q-factor versus frequency for $Ni_{0.8}Zn_{0.2}Fe_2O_4$ toroid

Conclusions:

For this project, nickel zinc ferrite annealed at temperature 900°C is chosen to be injected inside core sample. From the analysis of X-ray diffraction patterns, the single phase and good nanocrystalline of $Ni_{0.8}Zn_{0.2}Fe_2O_4$ particles were obtained at sintering temperature of 900 °C. It also has the best cubic ferrite crystallites with FESEM morphology dimension at 59nm to134nm. Moreover, due to low loss factor and high initial permeability $Ni_{0.8}Zn_{0.2}Fe_2O_4$ sintered at 900 °C has the best characteristics to be nanoparticles detector for oil recovery purposes.

4.3 Oil recovery using EM waves

4.3.1 Experiment 1: Porosity and Permeability Test for Core Sample.

This experiment was conducted in order to evaluate the core sample characteristics which are the porosity, pore volume and permeability. For the first step, the length and diameter of the core sample is measured using caliper. Then, the weight of the core sample is measured using balancer. After that, the core sample is placed into the porosimeter holder. Helium gas has been applied with high pressure. All the data are recorded after 30 minutes.

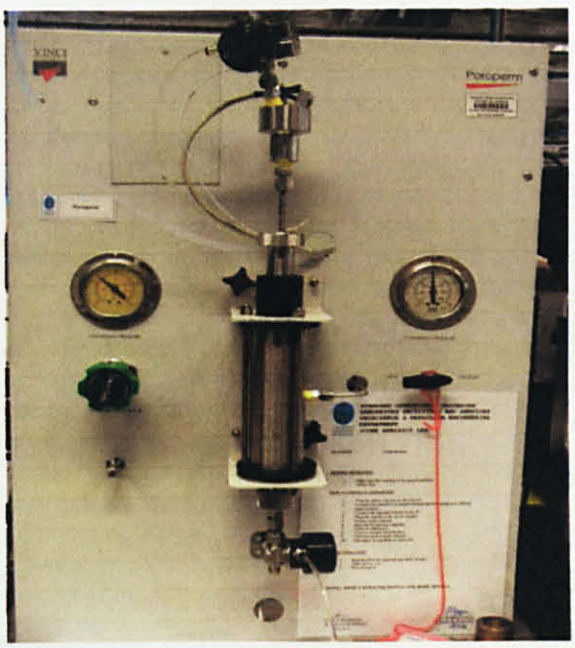

Figure 45: Helium Porosimeter

Results:

Table 7: Measurement from porosity test for core sample A1

Data	Measurement
Permeability(mD)	567.8002
Pore Volume V_p(cc)	17.7657
Porosity Φ (%)	21.1771
Grain Volume(cc)	66.1254
Bulk Volume(cc)	83.8910
Grain density(g/cc)	2.5940
Bulk density (g/cc)	2.0447

Table 8: Measurement from porosity test for core sample A2

Data	Measurement
Permeability(mD)	532.4349
Pore Volume V_p(cc)	18.2697
Porosity Φ (%)	20.7155
Grain Volume(cc)	70.0276
Bulk Volume(cc)	88.3243
Grain density(g/cc)	2.5730
Bulk density (g/cc)	2.0399

4.3.2 Experiment 2: Core Flooding

This experiment was conducted in order to prepare the core sample with crude oil and brine. For the second core, it has additional nickel zinc ferrite nanoparticle. For the first step, the core samples were saturate with the brine water for 24 hours. This procedure was to make sure that the core samples were fully saturated with the brine and there is no air inside the core. Vacuum pump is used to create the vacuum condition. Then, the core is weight and the weight of the core sample taken is called the weight before flooding.

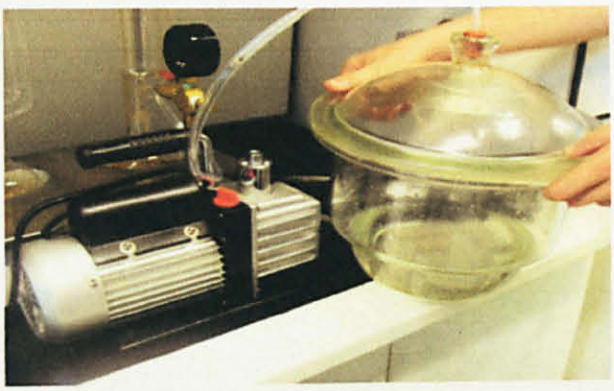

Figure 46: Vacuum pump for core saturation with brine water

Second step, the brine water with density of 1.018g/cc is injected again in the core sample using the core flooding machine to confirm that there was no air at all inside the core. For third step, the crude oil with density of 0.811g/cc is injected inside the core sample. The crude oil injection process was stopped once we noticed that there was no more brine water coming out at the outlet part. The oil that placed inside the core rock was calculated and called as the Original Oil in Place (OOIP).

Next step is second brine injection using the core flooding machine. This process was stopped once we notice that there was no more oil coming out from the outlet part. The remaining oil inside the core sample was calculated and it is called as

the Residue Oil in Place (ROIP). For the second core, one more step is added. Nanoparticle solution which consist of 0.6g nickel zinc ferrite nanoparticle and 200ml tab water been injected inside the core. The nanoparticle injection process was stopped once we noticed that there is crude oil comes out from the core sample. This shows the first recovery since nanoparticles have take over the oil place inside the core sample.

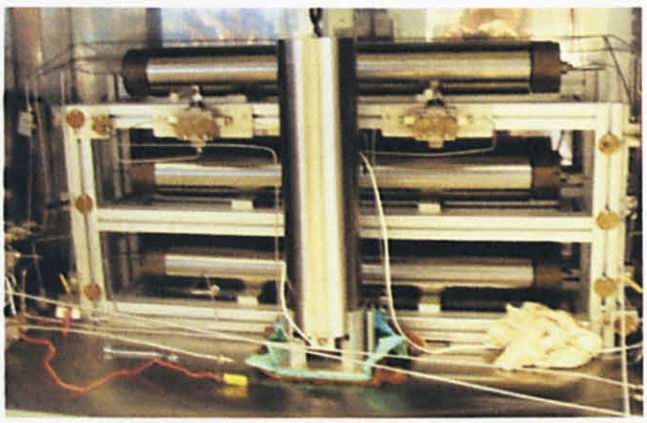

Figure 47: Core Flooding Machine

Results:

Table 9: Measurement after core flooding for core sample A1

Data	Measurement
Original oil in place OOIP (ml)	12
Residue oil in place ROIP (ml)	6.2

Table 10: Measurement after core flooding for core sample A2

Data	Measurement
Original oil in place OOIP (ml)	13
Residue oil in place ROIP (ml)	5

4.3.3 Experiment Setup

Condition 1: Without nanoparticle

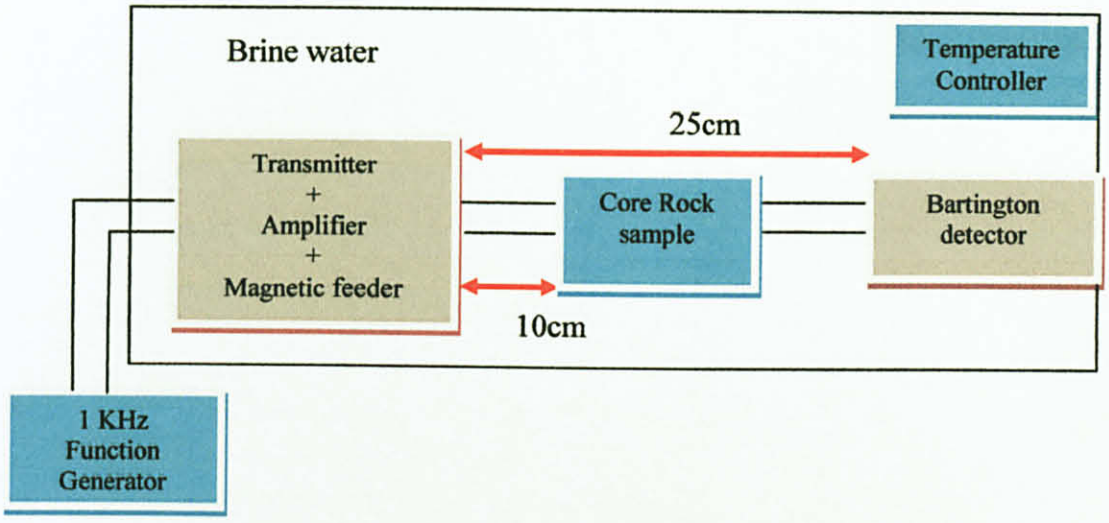

Figure 48: Basic setting using block diagram without nanoparticle

Condition 2: With nanoparticle

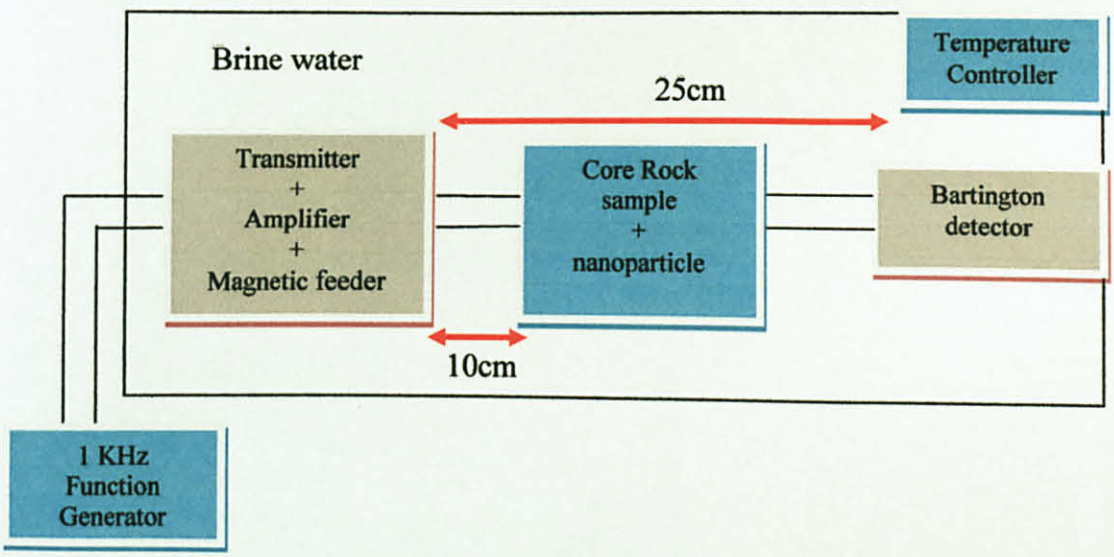

Figure 49: Basic setting using block diagram with nanoparticle

Figure above shows the basic set up of the experiment that been conduct in the lab. The 1 KHz function generator is used to supply AC current for transmitter. Nanoparticle magnetic feeder and amplifier is used to amplify the transmitted waves. At the same time, fluxgate magnetometer is used to measure the magnetic field which is transmitted by transmitter. Fluxgate magnetometer detector can also be used to analyze the percentage of recovered oil for the experiment. A conductive environment was created by filling the entire tank with saltwater which has density of 1.006g/cc. Temperature controller is used to increase and maintain the water temperature in the tank about 36°C - 37°C. The distance form transmitter to core rock sample and core rock sample to fluxgate magnetometer are fixed. Two separate experiments has been conduct with two different conditions. First experiment is using core sample without nanoparaticle while second experiment is using core sample with nanoparticle. The core sample was left to be exposed to the EM waves for 36 hours. Finally the percentage of oil recovery is calculated using weighting method. Results from both experiment were then been compared. Figure below shows the real experiment setup that been conducted in lab.

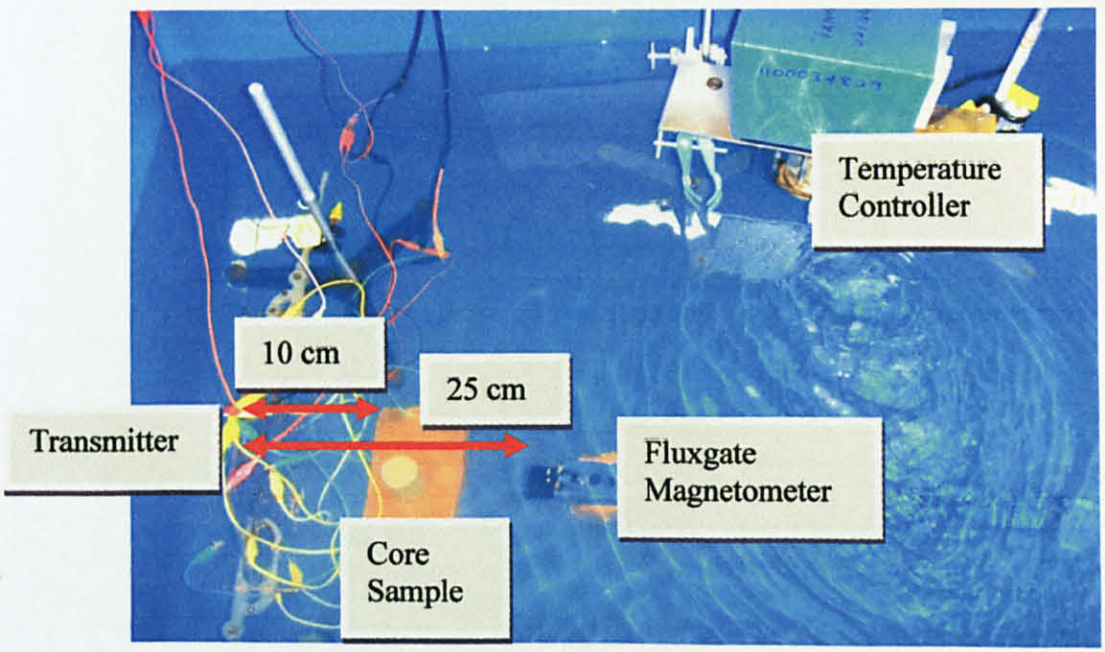

Figure 50: Experiment setup

4.3.4 Experiment 3

Objective:

To evaluate the percentage oil recovery for core rock sample without magnetic nanoparticle

Results from fluxgate magnetometer:

Table 11: Magnetic field (B field) distribution in different condition

Condition	Magnetic field (T)
Without rock	2.02E-08
Before flooding	2.02E-08
After flooding	4.20E-08

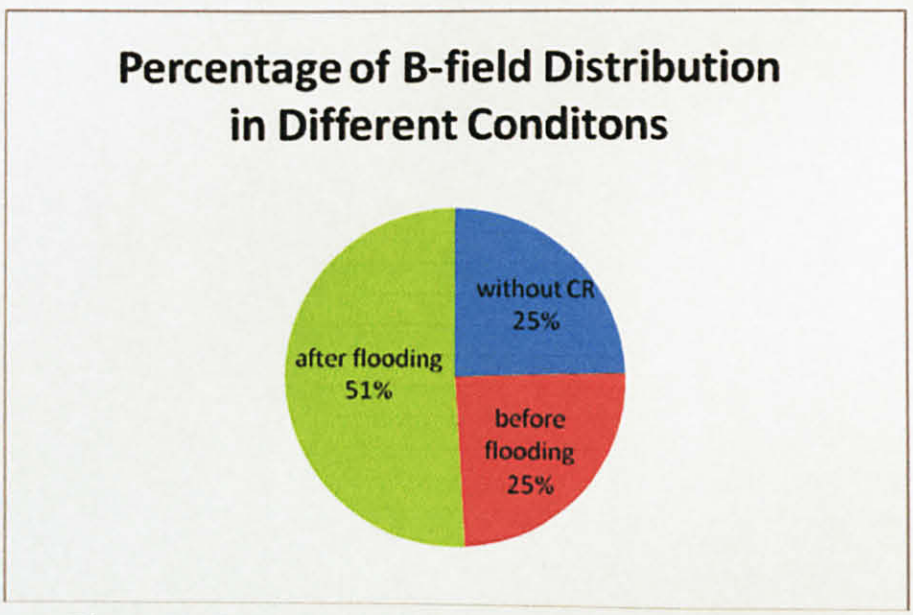

Figure 51: Percentage of B-field in different conditions

Discussion:

Pie chart shows that the percentage of B field for both conditions without and with empty core rock is the same which is 25%. However, the percentage of B field is higher for the flooded core sample. This shows that fluxgate magnetometer has detect the crude oil inside core rock samples

Table 12: Data of B field distribution through the core sample in 36 hours

Time	0 hr	2 hr	4 hr	10 hr	12 hr	18 hr	24 hr	36 hr
Magnetic field (T)	2.02E-08	3.77E-08	4.07E-08	4.20E-08	3.72E-08	3.44E-08	3.34E-08	3.33E-08

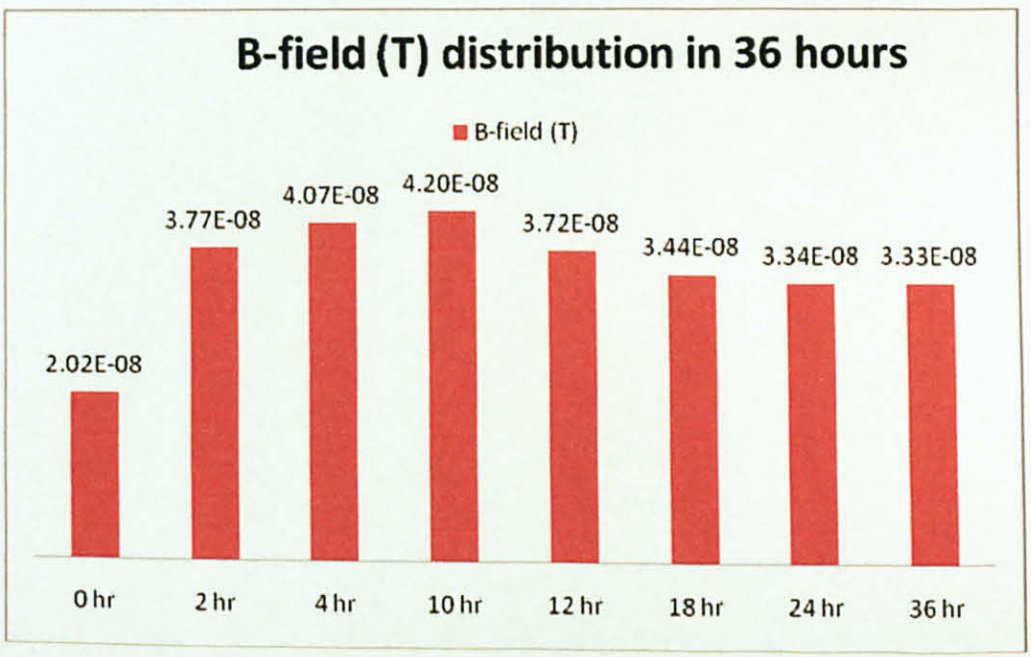

Figure 52: B field distribution through the core sample in 36 hours

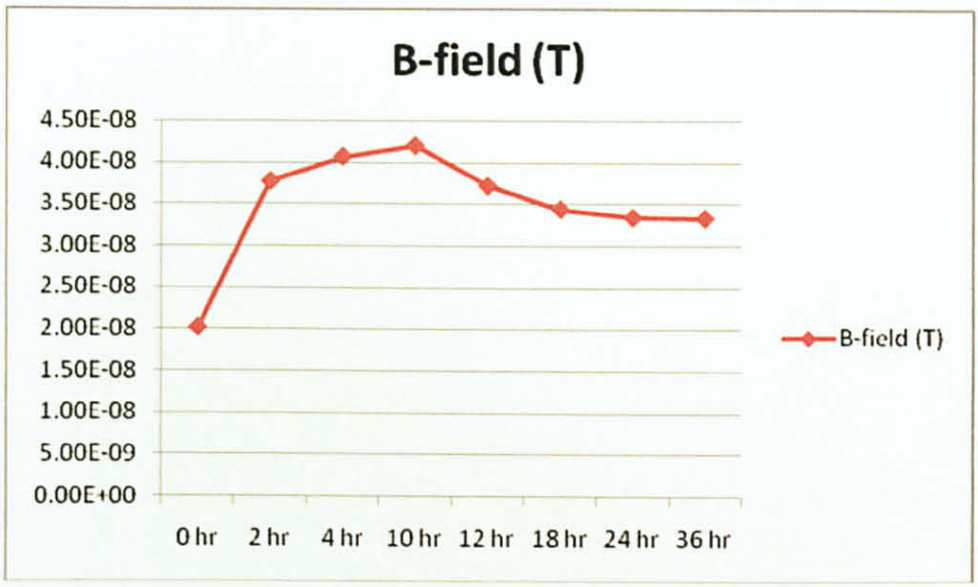

Figure 53: B field distribution through the core sample in 36 hours

Discussion:

From plotted graph, we can see that from 0 hours to 10 hours, the value of detection magnetic field is increasing from 2.02E-08 T to 4.20E-08 T. After 10 hours, the detection values start to decrease. This shows that there are some oil recovery after 10 hours, hence the value of detection magnetic field keep decreasing due to the oil that have been recovered.

Results from weighing method:

Table 13: Core sample data and measurements

Dry weight before flooding	173.535g
Weight after flooding	187.945g
Original Oil In Place (OOIP)	12ml
Produced oil after flooding	5.8ml
Residue Oil In Place (ROIP)	6.2ml
Weight after 36hours with EM waves	186.4g
Weight after dried in oven	177.321g

Calculation:

Remaining oil = Weight of core after dried in oven – weight of dry core before flooding

$$\text{Remaining Oil} = \frac{177.321g - 173.5354g}{0.811\frac{g}{ml}} = 4.67\text{ml}$$

Residue Oil in place (ROIP) = 6.2ml

Recovered Oil = Residue Oil in place - Remaining Oil

= 6.2ml-4.67ml = 1.53ml

$$\text{Recovery} = \frac{1.53ml}{12ml} X100 = 12.71\%\ \text{OOIP}$$

Discussion:

From calculation, the overall recovery for core sample A1 is 12.71% OOIP. However, the percent of recovery is not accurate because amount of water inside the core is not been measured.

4.3.5 Experiment 4

Objective:

To evaluate the percentage of oil recovery for core rock sample with magnetic nanoparticle

Results from fluxgate magnetometer:

Table 14: Magnetic field (B field) distribution in different condition

Condition	Magnetic field (T)
Without rock	2.02E-08
Before flooding	2.02E-08
After flooding	4.00E-08

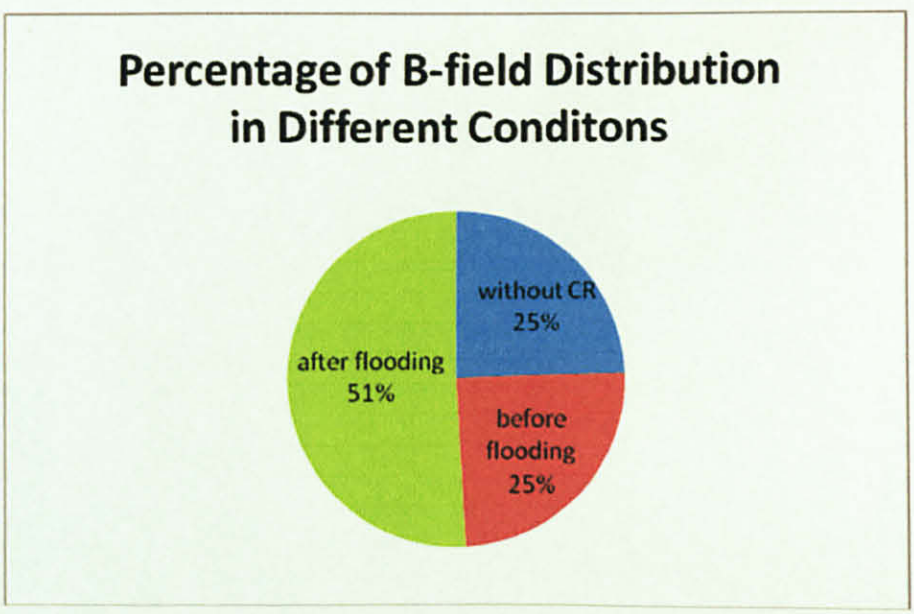

Figure 54: Percentage of B-field in different conditions

Discussion:

Pie chart shows that the percentage of B field for both conditions without and with empty core rock is the same which is 25%. However, the percentage of B field is higher for the flooded core sample. This shows that fluxgate magnetometer has detect the crude oil inside core rock samples

Table 15: Data of B field distribution through the core sample in 36 hours

Time	**0 hr**	**2 hr**	**4 hr**	**6 hr**	**12 hr**	**18 hr**	**24 hr**	**36 hr**
Magnetic field (T)	2.02E-08	3.50E-08	3.57E-08	3.75E-08	4.00E-08	3.76E-08	3.61E-08	3.61E-08

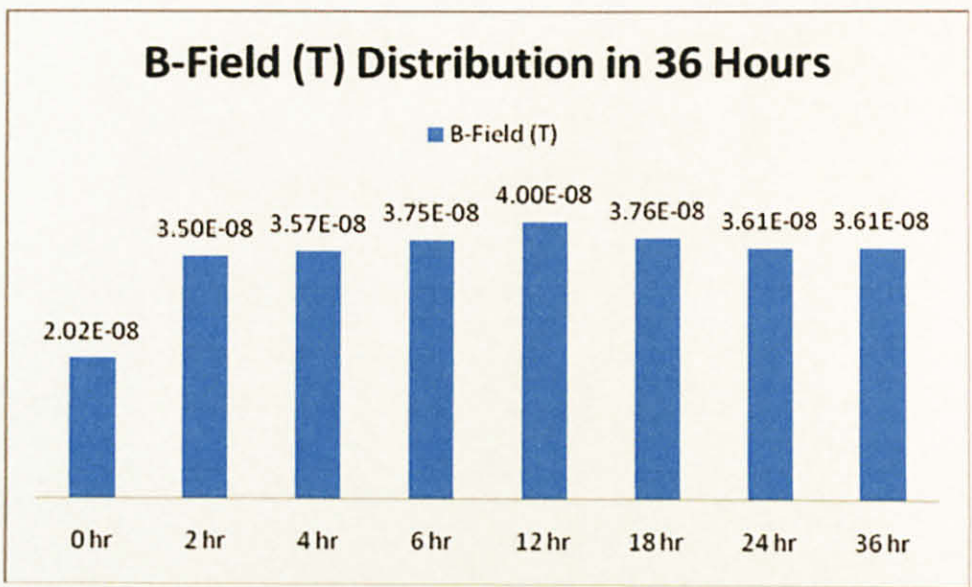

Figure 55: B field distribution through the core sample in 36 hours

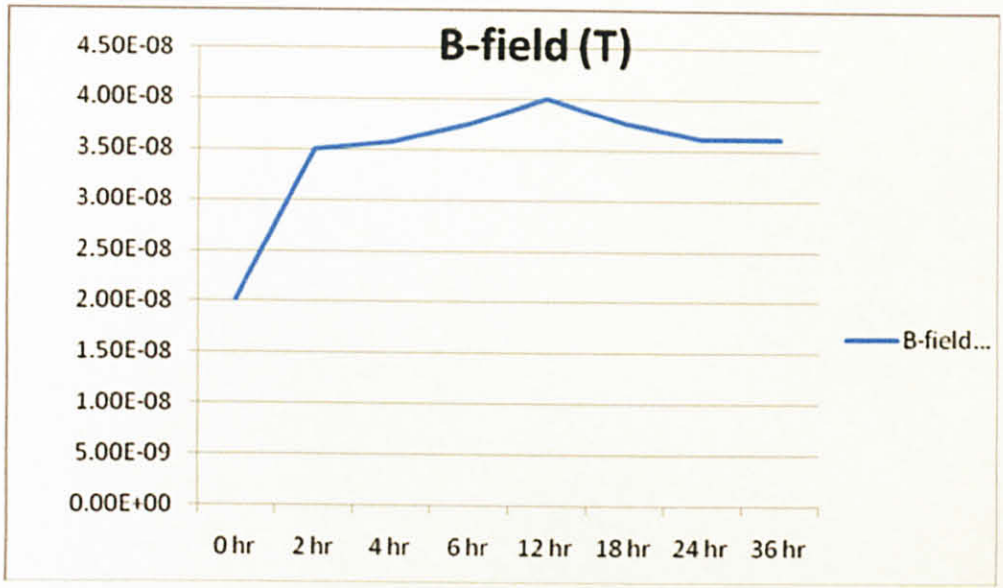

Figure 56: B field distribution through the core sample in 36 hours

Discussion:

A previous result shows that fluxgate magnetometer can detect the existence of crude oil inside core rock samples. From plotted graph, we can see that from 0 hours to 12 hours, the value of detection magnetic field is increasing from 2.02E-08 T to 4.00E-08 T. After 12 hours, the detection values start to decrease. At 24 to 36 hours, the values of detection magnetic field remain the same at 3.61E-08. This shows that there are some oil recovery after 12 hours, hence the value of detection magnetic field keep decreasing due to the oil that have been recovered.

Results from weighing method:

Table 16: Core sample data and measurements

	Dry weight before flooding	180.1993g
	Weight after flooding before adding nanoparticle	196.6g
	Original Oil In Place (OOIP)	13ml
	Produced oil after flooding	8ml
	Residue Oil In Place (ROIP)	5ml
	Weight after adding nanoparticle	194.911g
	Oil produced after flushing nanoparticle	0.6ml
	Weight of nanoparticle used	0.4866g
	Weight after 36hours with EM wave	193.73g
	Weight after dried in oven	182.235g

Calculation:

Remaining oil = Weight of core after dried in oven –weight of dry core before flooding – weight of nanoparticle used

$$\text{Remaining Oil} = \frac{182.235g - 180.1993g - 0.4866g}{0.811\frac{g}{ml}} = 1.918\text{ml}$$

Residue Oil in place (ROIP) = 5ml

Recovered Oil = Residue Oil in place - Remaining Oil

= 5ml-1.918ml

= 3.082ml

$$\text{Recovery} = \frac{3.082ml}{13ml} X100 = 23.7\%\ \text{OOIP}$$

Discussion:

For core sample A2, about 0.48 g nanoparticles is injected to the core sample during core flooding process. During the flushing of nanoparticle, about 0.6 ml oil comes out from the core sample. This shows that the nanoparticles have take over the oil place inside the core sample. From calculation, the overall recovery for core sample A2 is 23.7% OOIP. However, the percent of recovery is not accurate because amount of water inside the core is not been measured.

4.3.6 Comparison between recovery of core sample A1 and A2 against time

Table 17: Comparison between core sample A1 and A2

Core sample	A1 (Without nanoparticle)	A2 (With nanoparticle)
After 12 hours		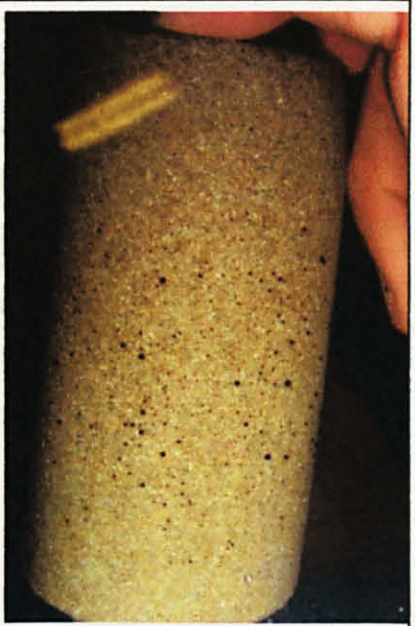
After 18 hours		

Core sample	A1 (Without nanoparticle)	A2 (With nanoparticle)
After 24 hours		
After 36 hours		

Discussion:

Figure on the above table shows that comparison between oil recovery for both core samples A1 and A2 against time. At 12 hours, oil is started to come out for core sample A2. On the other hand, it takes about 18 hours for oil to come out at core sample A1. After that, oil are continuously been recovered for both core samples A1 and A2 until 36 hours. The percentage of the oil recovery is calculated using weighting method,

From this experiment, it is proven that 1 KHz of frequency is sufficient enough to recover oil from the core sample. Moreover, by adding magnetic nanoparticle to the core sample, it will enhance more oil recovery. This is because magnetic nanoparticle's like nickel zinc ferrite can be the medium to absorb EM waves and also assist the oil recovery at the same time. From calculation, results shows that by adding nanoparticle to the core sample, 23.7% OOIP of oil can be recover compared to only 12.7% OOIP without using nanoparticle.

CHAPTER 5

CONCLUSION & RECOMMENDATION

5.1 Conclusion

Nickel zinc ferrite nanoparticle was successfully synthesized using sol gel methods. $Ni_{0.8}Zn_{0.2}Fe_2O_4$ nanoparticles prepared at low temperature exhibit good crystal structure, fine grain size and good magnetic properties. Through this project, we had successfully recovered about 23.7% of oil using magnetic nanoparticle compared to only 12.7% of oil without magnetic nanoparticle using EM methods. This method is the first conducted in UTP and PETRONAS. By using only 1 KHz supply, oil can be recovered. Therefore,it is proven that magnetic nanoparticle's like nickel zinc ferrite can be the medium to absorb EM waves and also assist the oil recovery at the same time. Therefore, nanoparticle can be one of the EOR alternatives in order to improve the crude oil production.

The first major finding in this project is the magnetic nanoparticles. Nano sized magnetic nanoparticle which is nickel zinc ferrite ($Ni_{0.8}Zn_{0.2}Fe_2O_4$) have been successfully synsthesized using sol gel technique. By using XRD characterization, the highest peak intensity is observed for [3 1 1] plane at 2-theta. The particle sizes are in the range of 35.06 nm to 106.99 nm calculated using Scherer's equation. Morphology of nanostructure and dimension of grain size for nickel zinc ferrite nanoparticle is clearly seen using FESEM. FESEM results show the grain size of nanoparticle which

is in range of 50nm-150nm. Energy Dispersive X-Ray (EDX) is performed in conjunction with FESEM. Result obtain shows that the atomic and weight percentage of the corresponding elements which are Nickel, Zinc, Ferum and Oxygen. By performing magnetic characterization, result shows that nickel zinc ferrite have good permeability, high quality factor and low relative loss factor.

Second major finding is the nanoparticle magnetic feeder. Result shows that nanoparticle feeder has increase about 25.6% of transmitted EM waves compared to use the transmitter without nanoparticle feeder. Therefore, nickel zinc ferrite is suitable to use as a feeder for transmitter.

5.2 Recommendation

There are lots parameter can be changes in order to improve the project and get more accurate results. Below are some recommendations:

1. Change the synthesis methods from sol gel to self combustion methods.
2. Decrease the size of nanoparticles by using ultrasonic bath.
3. Change the ratio of nickel and zinc in order to synthesis nickel zinc ferrite. For this project, $Ni_{0.8}Zn_{0.2}Fe_2O_4$ is used.
4. Ensure that particle size is about the same to make sure all particles can be suspended in water during core flooding.
5. Instead of using magnetic nanoparticle like nickel zinc ferrite, we can also use electric naoparticle like zinc oxide and aluminium oxide.
6. Decreased the size of transmitter and water tank.
7. Varies the distance between core rock sample, transmitter and decaport.

REFERENCES

[1] A.G.Nutan, C.V.Subhash and D.C.Kashyap: *Solid State Commun.,* 2005, 134, 689.

[2] K.H.Wu, W.C.Huang, G.P. Wang and T.R.Wu: *Mater. Res. Bull.,* 2005, 40, 1822.

[3] http://en.wikipedia.org/wiki/Enhanced_oil_recovery

[4] http://pubs.acs.org/cen/government/85/8539gov1.htm

[5] Q. Song, Z. J. Zhang, "Shape control and associated magnetic properties of spinel Cobalt ferrite nanocrystals" J. Am. Chem. Soc., vol.126, pp. 6164-6168 Apr. 2004

[6] Shah, Ruxheet D (2009). Application of nanoparticle saturated injectant gases for EOR of heavy Oils. SPE October 2009

[7] V N Paunov, G Mackenzie and S D Stoyanov, *J. Mater. Chem.*, 2007

[8] Costa ACFM, Tortella E, Morelli MR, Kiminami RHGA (2003) Mater Sci Forum 416–418:699

[9] D.H. Chen, X.R. He / Materials Research Bulletin 36 (2001) 1369–1377

[10] Islam, M. R., and Chakma, A. (1992). A new recovery technique for heavy-oil reservoirs with bottomwater. SPE 20258. Product. Eng. May, 1992.

[11] Chakma, A., and Jha, K. N. (1992). Heavy oil recovery from thin pay zones by electromagnetic heating. SPE Paper 24817. 67th Annual Technical Conference and Exhibition, Washington, DC, October 4–7.

[12] Bjorndalen, N., Mustafiz, S., and Islam, M. R. (2005). The effect of irradiation on immiscible fluids for increased oil production with horizontal wells. Proceedings of IMECE 2005 ASME International Mechanical Engineering Congress and Exposition, Orlando, FL, November 5–11,IMECE2005-81752

[13] http://en.wikipedia.org/wiki/Electromagnetic_radiation

[14] http://electricitymagnetism.suite101.com/article.cfm/understanding_lenzs_law

[15] http://www.russia-ic.com/education_science/education/gems/809/

[16] Azároff, L. R. Kaplow, N. Kato, R. J. Weiss, A. J. C. Wilson, R. A. Young (1974). *X-ray diffraction*. McGraw-Hill

[17] http://www.photometrics.net/fesem.html

[18] http://en.wikipedia.org/wiki/X-ray_scattering_techniques, (2009)

[19] H. P. Klung, L. E. Alexander, "X-ray diffraction procedure for polycrystalline procedure for polycrystalline and amorphous materials", wiley, New York 1974.

[20] A. Verma, T.C. Geol, R.G. Mendiratta and P. Kishon, "Magnetic properties of nickel–zinc ferrites prepared by the citrate precursor method", J. Magn. Magn. Mater., vol. 208, pp. 13-19, Jan. 2000

[21] P.K.Roy, J.Bera, "Characterization of nanocrystalline NiCuZn ferrite powder synthesized by solgel auto combustion method", J.Mat.Proc.Tech, Vol197,(2008),pp.279-283

[22] Fawwaz T.Ulaby, Magnetostatics, Electromagnetics for Engineers, Pearson Education International, The University of Michigan, (2005)

APPENDIX

- Data for Core rock sample A1

Table 1: B field transmitted without core rock

without rock_1	without rock_2	without rock_2	avg
1.86E-08	1.40E-08	2.08E-08	1.78E-08
2.24E-08	1.92E-08	1.62E-08	1.93E-08
2.63E-08	2.35E-08	9.93E-09	1.99E-08
2.79E-08	2.63E-08	4.06E-09	1.94E-08
2.81E-08	2.78E-08	8.54E-09	2.15E-08
2.81E-08	2.83E-08	1.40E-08	2.34E-08
2.74E-08	2.75E-08	1.94E-08	2.48E-08
2.49E-08	2.48E-08	2.41E-08	2.46E-08
2.27E-08	2.07E-08	2.69E-08	2.34E-08
1.83E-08	1.48E-08	2.80E-08	2.04E-08
1.29E-08	8.17E-09	2.88E-08	1.66E-08
7.43E-09	5.30E-09	2.81E-08	1.36E-08
4.75E-09	1.21E-08	2.58E-08	1.42E-08
1.05E-08	1.77E-08	2.32E-08	1.71E-08
1.55E-08	2.25E-08	1.83E-08	1.88E-08
2.06E-08	2.66E-08	1.32E-08	2.01E-08
2.39E-08	2.81E-08	6.78E-09	1.96E-08
2.66E-08	2.81E-08	5.36E-09	2.00E-08
2.79E-08	2.76E-08	1.09E-08	2.21E-08
2.83E-08	2.60E-08	1.66E-08	2.36E-08
2.77E-08	2.21E-08	2.13E-08	2.37E-08
			2.02E-08

Table 2: B field transmitted through core before flooding

before flooding_1	before flooding_2	before flooding_3	avg
2.52E-08	1.41E-08	2.40E-08	2.11E-08
2.75E-08	7.73E-09	2.73E-08	2.08E-08
2.75E-08	1.81E-08	9.93E-09	1.85E-08
2.44E-08	2.46E-08	4.06E-09	1.77E-08
1.74E-08	2.74E-08	8.54E-09	1.78E-08
9.12E-09	2.79E-08	1.40E-08	1.70E-08
1.31E-08	2.62E-08	1.94E-08	1.96E-08
2.11E-08	2.01E-08	1.96E-08	2.03E-08
2.63E-08	1.11E-08	2.51E-08	2.08E-08
2.73E-08	9.94E-09	2.77E-08	2.16E-08
2.72E-08	1.93E-08	2.75E-08	2.47E-08
2.33E-08	2.51E-08	2.54E-08	2.46E-08
1.53E-08	2.81E-08	1.84E-08	2.06E-08
5.87E-09	2.74E-08	8.79E-09	1.40E-08
1.60E-08	2.51E-08	1.34E-08	1.82E-08
2.35E-08	1.82E-08	2.08E-08	2.08E-08
2.70E-08	9.12E-09	2.66E-08	2.09E-08
2.77E-08	1.18E-08	2.75E-08	2.23E-08
2.58E-08	2.07E-08	2.70E-08	2.45E-08
2.06E-08	2.62E-08	2.30E-08	2.33E-08
1.18E-08	2.80E-08	1.50E-08	1.83E-08
			2.04E-08

Table 3: B field transmitted through core after flooding

after flooding1	after flooding2	after flooding3	avg
4.62E-08	4.52E-08	4.58E-08	4.57E-08
4.33E-08	4.64E-08	4.24E-08	4.40E-08
3.97E-08	2.92E-08	4.16E-08	3.68E-08
4.67E-08	4.57E-08	4.61E-08	4.62E-08
4.02E-08	4.52E-08	3.74E-08	4.09E-08
4.27E-08	3.48E-08	4.39E-08	4.05E-08
4.62E-08	4.60E-08	4.60E-08	4.61E-08
3.38E-08	4.38E-08	3.08E-08	3.61E-08
4.52E-08	3.99E-08	4.54E-08	4.35E-08
4.62E-08	4.62E-08	4.56E-08	4.60E-08
2.99E-08	4.04E-08	3.22E-08	3.42E-08
4.60E-08	4.26E-08	4.61E-08	4.49E-08
4.44E-08	4.62E-08	4.49E-08	4.52E-08
3.69E-08	3.42E-08	3.74E-08	3.62E-08
4.57E-08	4.58E-08	4.00E-08	4.38E-08
4.28E-08	4.64E-08	4.24E-08	4.39E-08
4.21E-08	2.83E-08	4.07E-08	3.70E-08
4.60E-08	4.57E-08	4.00E-08	4.39E-08
3.81E-08	4.58E-08	3.74E-08	4.04E-08
4.37E-08	3.47E-08	4.38E-08	4.07E-08
4.63E-08	4.60E-08	4.58E-08	4.60E-08
			4.20E-08

Table 4: B field transmitted through core after 2 hours

2hours_1	2hours_2	2hours_3	avg
4.50E-08	4.55E-08	3.57E-08	4.21E-08
4.51E-08	4.10E-08	2.05E-08	3.55E-08
3.44E-08	2.50E-08	3.88E-08	3.27E-08
2.33E-08	3.32E-08	4.56E-08	3.40E-08
3.92E-08	4.53E-08	4.50E-08	4.32E-08
4.54E-08	4.55E-08	3.65E-08	4.25E-08
4.46E-08	4.04E-08	1.96E-08	3.49E-08
3.36E-08	2.37E-08	3.71E-08	3.15E-08
2.35E-08	3.43E-08	4.50E-08	3.43E-08
4.04E-08	4.49E-08	4.53E-08	4.35E-08
4.52E-08	4.59E-08	3.75E-08	4.29E-08
4.39E-08	3.98E-08	2.12E-08	3.50E-08
3.34E-08	2.32E-08	3.62E-08	3.09E-08
2.45E-08	3.55E-08	4.53E-08	3.51E-08
4.07E-08	4.51E-08	4.54E-08	4.37E-08
4.55E-08	4.55E-08	3.95E-08	4.35E-08
4.44E-08	3.86E-08	2.26E-08	3.52E-08
3.32E-08	2.10E-08	3.49E-08	2.97E-08
2.45E-08	3.64E-08	4.48E-08	3.52E-08
4.09E-08	4.48E-08	4.53E-08	4.37E-08
4.50E-08	4.52E-08	4.04E-08	4.35E-08
			3.77E-08

Table 5: B field transmitted through core after 4 hours

4hours_1	4hours_2	4hours_3	avg
4.18E-08	4.54E-08	4.33E-08	4.35E-08
4.57E-08	4.46E-08	4.59E-08	4.54E-08
3.83E-08	2.67E-08	3.31E-08	3.27E-08
4.11E-08	4.53E-08	4.40E-08	4.35E-08
4.56E-08	4.47E-08	4.60E-08	4.54E-08
3.82E-08	2.83E-08	3.35E-08	3.33E-08
4.22E-08	4.49E-08	4.34E-08	4.35E-08
4.53E-08	4.48E-08	4.57E-08	4.53E-08
3.74E-08	2.97E-08	3.21E-08	3.31E-08
4.22E-08	4.53E-08	4.50E-08	4.42E-08
4.49E-08	4.54E-08	4.58E-08	4.54E-08
3.66E-08	2.96E-08	3.18E-08	3.27E-08
4.21E-08	4.50E-08	4.37E-08	4.36E-08
4.52E-08	4.44E-08	4.55E-08	4.50E-08
3.70E-08	3.18E-08	3.10E-08	3.33E-08
4.23E-08	4.57E-08	4.49E-08	4.43E-08
4.53E-08	4.50E-08	4.53E-08	4.52E-08
3.69E-08	3.29E-08	2.98E-08	3.32E-08
4.32E-08	4.56E-08	4.37E-08	4.42E-08
4.48E-08	4.47E-08	4.54E-08	4.50E-08
3.67E-08	3.31E-08	3.06E-08	3.35E-08
			4.07E-08

Table 6: B field transmitted through core after 10 hours

10hours_1	10hours_2	10hours_3	avg
4.62E-08	4.52E-08	4.58E-08	4.57E-08
4.33E-08	4.64E-08	4.24E-08	4.40E-08
3.97E-08	2.92E-08	4.16E-08	3.68E-08
4.67E-08	4.57E-08	4.61E-08	4.62E-08
4.02E-08	4.52E-08	3.74E-08	4.09E-08
4.27E-08	3.48E-08	4.39E-08	4.05E-08
4.62E-08	4.60E-08	4.60E-08	4.61E-08
3.38E-08	4.38E-08	3.08E-08	3.61E-08
4.52E-08	3.99E-08	4.54E-08	4.35E-08
4.62E-08	4.62E-08	4.56E-08	4.60E-08
2.99E-08	4.04E-08	3.22E-08	3.42E-08
4.60E-08	4.26E-08	4.61E-08	4.49E-08
4.44E-08	4.62E-08	4.49E-08	4.52E-08
3.69E-08	3.42E-08	3.74E-08	3.62E-08
4.57E-08	4.58E-08	4.00E-08	4.38E-08
4.28E-08	4.64E-08	4.24E-08	4.39E-08
4.21E-08	2.83E-08	4.07E-08	3.70E-08
4.60E-08	4.57E-08	4.00E-08	4.39E-08
3.81E-08	4.58E-08	3.74E-08	4.04E-08
4.37E-08	3.47E-08	4.38E-08	4.07E-08
4.63E-08	4.60E-08	4.58E-08	4.60E-08
			4.20E-08

Table 7: B field transmitted through core after 12 hours

12 hours_1	12 hours_2	12 hours_3	Avg
2.33E-08	4.35E-08	3.05E-08	3.24E-08
3.75E-08	3.22E-08	4.26E-08	3.75E-08
4.41E-08	2.86E-08	4.45E-08	3.91E-08
4.36E-08	4.18E-08	4.04E-08	4.19E-08
3.43E-08	4.39E-08	2.63E-08	3.48E-08
2.50E-08	4.24E-08	3.40E-08	3.38E-08
4.05E-08	2.68E-08	4.37E-08	3.70E-08
4.43E-08	3.31E-08	4.41E-08	4.05E-08
4.35E-08	4.38E-08	3.90E-08	4.21E-08
2.93E-08	4.44E-08	2.34E-08	3.23E-08
3.21E-08	3.94E-08	3.68E-08	3.61E-08
4.32E-08	2.37E-08	4.41E-08	3.70E-08
4.43E-08	3.76E-08	4.44E-08	4.21E-08
3.92E-08	4.44E-08	3.64E-08	4.00E-08
2.43E-08	4.40E-08	2.41E-08	3.08E-08
3.62E-08	3.40E-08	3.86E-08	3.63E-08
4.37E-08	2.58E-08	4.48E-08	3.81E-08
4.44E-08	4.04E-08	4.42E-08	4.30E-08
3.54E-08	4.46E-08	3.32E-08	3.78E-08
2.57E-08	4.33E-08	2.71E-08	3.20E-08
3.99E-08	3.12E-08	4.11E-08	3.74E-08
			3.72E-08

Table 8: B field transmitted through core after18 hours

18 hours_1	18 hours_2	18 hours_3	avg
3.68E-08	3.49E-08	4.02E-08	3.73E-08
2.70E-08	2.59E-08	4.02E-08	3.10E-08
2.89E-08	3.02E-08	3.55E-08	3.15E-08
3.71E-08	3.76E-08	2.62E-08	3.36E-08
4.02E-08	4.09E-08	3.03E-08	3.71E-08
3.95E-08	3.92E-08	3.78E-08	3.88E-08
3.43E-08	3.26E-08	4.04E-08	3.58E-08
2.49E-08	2.40E-08	3.98E-08	2.96E-08
3.11E-08	3.21E-08	3.26E-08	3.19E-08
3.89E-08	3.88E-08	2.45E-08	3.41E-08
4.04E-08	4.05E-08	3.28E-08	3.79E-08
3.91E-08	3.82E-08	4.00E-08	3.91E-08
3.10E-08	3.03E-08	4.00E-08	3.38E-08
2.46E-08	2.62E-08	3.81E-08	2.96E-08
3.41E-08	3.46E-08	2.95E-08	3.27E-08
4.05E-08	3.99E-08	2.63E-08	3.56E-08
4.07E-08	4.09E-08	3.51E-08	3.89E-08
3.76E-08	3.60E-08	4.07E-08	3.81E-08
2.81E-08	2.71E-08	4.03E-08	3.18E-08
2.73E-08	2.85E-08	3.65E-08	3.08E-08
3.65E-08	3.75E-08	2.68E-08	3.36E-08
			3.44E-08

Table 9: B field transmitted through core after 24 hours

24 hours_1	24 hours_2	24 hours_3	avg
3.63E-08	3.56E-08	3.07E-08	3.42E-08
3.61E-08	3.63E-08	3.61E-08	3.62E-08
3.24E-08	3.43E-08	3.69E-08	3.45E-08
2.82E-08	2.67E-08	3.26E-08	2.92E-08
3.56E-08	3.35E-08	2.73E-08	3.21E-08
3.62E-08	3.63E-08	3.44E-08	3.56E-08
3.46E-08	3.57E-08	3.61E-08	3.55E-08
2.76E-08	2.91E-08	3.49E-08	3.05E-08
3.24E-08	3.15E-08	2.81E-08	3.07E-08
3.69E-08	3.59E-08	3.21E-08	3.50E-08
3.54E-08	3.63E-08	3.65E-08	3.61E-08
3.00E-08	3.14E-08	3.64E-08	3.26E-08
3.00E-08	2.90E-08	3.13E-08	3.01E-08
3.59E-08	3.55E-08	2.97E-08	3.37E-08
3.66E-08	3.76E-08	3.58E-08	3.67E-08
3.33E-08	3.38E-08	3.62E-08	3.44E-08
2.72E-08	2.71E-08	3.37E-08	2.93E-08
3.50E-08	3.41E-08	2.70E-08	3.20E-08
3.61E-08	3.65E-08	3.40E-08	3.55E-08
3.50E-08	3.56E-08	3.64E-08	3.57E-08
2.91E-08	2.86E-08	3.63E-08	3.13E-08
			3.34E-08

Table 10: B field transmitted through core after 36 hours

36 hours_1	36 hours_2	36 hours_3	avg
3.38E-08	3.63E-08	3.36E-08	3.46E-08
3.55E-08	3.44E-08	3.54E-08	3.51E-08
3.30E-08	2.78E-08	3.37E-08	3.15E-08
2.95E-08	3.58E-08	2.94E-08	3.16E-08
3.59E-08	3.58E-08	3.62E-08	3.60E-08
3.59E-08	3.09E-08	3.62E-08	3.43E-08
2.94E-08	3.26E-08	3.03E-08	3.08E-08
3.33E-08	3.61E-08	3.26E-08	3.40E-08
3.60E-08	3.60E-08	3.65E-08	3.62E-08
3.42E-08	2.70E-08	3.37E-08	3.16E-08
2.88E-08	3.46E-08	2.82E-08	3.05E-08
3.54E-08	3.58E-08	3.52E-08	3.55E-08
3.58E-08	3.28E-08	3.55E-08	3.47E-08
2.94E-08	3.06E-08	3.09E-08	3.03E-08
3.33E-08	3.61E-08	3.21E-08	3.38E-08
3.57E-08	3.58E-08	3.62E-08	3.59E-08
3.41E-08	2.88E-08	3.47E-08	3.25E-08
2.90E-08	3.44E-08	2.70E-08	3.01E-08
3.58E-08	3.59E-08	3.50E-08	3.56E-08
3.59E-08	3.32E-08	3.59E-08	3.50E-08
3.02E-08	2.91E-08	3.20E-08	3.04E-08
			3.33E-08

- Data for Core rock sample A2

Table 11: B field transmitted without core rock

without rock_1	without rock_2	without rock_3	avg
1.86E-08	1.40E-08	2.08E-08	1.78E-08
2.24E-08	1.92E-08	1.62E-08	1.93E-08
2.63E-08	2.35E-08	9.93E-09	1.99E-08
2.79E-08	2.63E-08	4.06E-09	1.94E-08
2.81E-08	2.78E-08	8.54E-09	2.15E-08
2.81E-08	2.83E-08	1.40E-08	2.34E-08
2.74E-08	2.75E-08	1.94E-08	2.48E-08
2.49E-08	2.48E-08	2.41E-08	2.46E-08
2.27E-08	2.07E-08	2.69E-08	2.34E-08
1.83E-08	1.48E-08	2.80E-08	2.04E-08
1.29E-08	8.17E-09	2.88E-08	1.66E-08
7.43E-09	5.30E-09	2.81E-08	1.36E-08
4.75E-09	1.21E-08	2.58E-08	1.42E-08
1.05E-08	1.77E-08	2.32E-08	1.71E-08
1.55E-08	2.25E-08	1.83E-08	1.88E-08
2.06E-08	2.66E-08	1.32E-08	2.01E-08
2.39E-08	2.81E-08	6.78E-09	1.96E-08
2.66E-08	2.81E-08	5.36E-09	2.00E-08
2.79E-08	2.76E-08	1.09E-08	2.21E-08
2.83E-08	2.60E-08	1.66E-08	2.36E-08
2.77E-08	2.21E-08	2.13E-08	2.37E-08
			2.02E-08

Table 12: B field transmitted through core before flooding

before flooding_1	before flooding_2	before flooding_3	avg
2.37E-08	1.67E-08	6.85E-09	1.58E-08
2.73E-08	2.47E-08	1.76E-08	2.32E-08
2.70E-08	2.70E-08	2.44E-08	2.61E-08
2.35E-08	2.71E-08	2.66E-08	2.57E-08
1.49E-08	2.29E-08	2.61E-08	2.13E-08
1.04E-08	1.33E-08	2.15E-08	1.51E-08
2.07E-08	1.03E-08	1.23E-08	1.45E-08
2.63E-08	2.05E-08	1.24E-08	1.97E-08
2.71E-08	2.63E-08	2.14E-08	2.50E-08
2.51E-08	2.71E-08	2.59E-08	2.60E-08
1.85E-08	2.57E-08	2.67E-08	2.36E-08
7.86E-09	2.00E-08	2.50E-08	1.76E-08
1.71E-08	9.95E-09	1.71E-08	1.47E-08
2.43E-08	1.41E-08	7.09E-09	1.51E-08
2.68E-08	2.29E-08	1.77E-08	2.25E-08
2.64E-08	2.72E-08	2.48E-08	2.61E-08
2.18E-08	2.73E-08	2.72E-08	2.54E-08
1.28E-08	2.37E-08	2.63E-08	2.09E-08
1.20E-08	1.57E-08	2.17E-08	1.65E-08
2.15E-08	7.84E-09	1.27E-08	1.40E-08
2.65E-08	1.86E-08	1.16E-08	1.89E-08
			2.04E-08

Table 13: B field transmitted through core after flooding

after flooding_1	after flooding_2	after flooding_3	avg
4.02E-08	3.97E-08	4.00E-08	4.00E-08
4.01E-08	4.07E-08	4.03E-08	4.03E-08
3.95E-08	3.97E-08	3.99E-08	3.97E-08
4.05E-08	4.04E-08	4.00E-08	4.03E-08
3.96E-08	3.95E-08	3.94E-08	3.95E-08
4.02E-08	4.00E-08	4.00E-08	4.01E-08
3.97E-08	3.96E-08	4.03E-08	3.99E-08
3.95E-08	3.96E-08	3.99E-08	3.97E-08
4.00E-08	4.03E-08	4.00E-08	4.01E-08
4.04E-08	4.01E-08	3.94E-08	4.00E-08
4.02E-08	3.97E-08	4.00E-08	3.99E-08
4.01E-08	4.01E-08	4.03E-08	4.02E-08
4.01E-08	4.02E-08	3.99E-08	4.01E-08
3.98E-08	3.99E-08	4.00E-08	3.99E-08
4.01E-08	4.02E-08	3.94E-08	3.99E-08
3.98E-08	4.00E-08	4.00E-08	4.00E-08
4.06E-08	4.05E-08	4.03E-08	4.05E-08
4.06E-08	3.99E-08	3.99E-08	4.01E-08
4.03E-08	4.00E-08	4.00E-08	4.01E-08
4.01E-08	3.95E-08	3.94E-08	3.97E-08
4.01E-08	4.02E-08	4.00E-08	4.01E-08
			4.00E-08

Table 14: B field transmitted through core after 2 hours

2hours_1	2hours_2	2hours_3	avg
3.61E-08	3.08E-08	3.64E-08	3.44E-08
3.09E-08	3.79E-08	3.79E-08	3.55E-08
3.74E-08	3.74E-08	3.05E-08	3.51E-08
3.61E-08	2.96E-08	3.68E-08	3.41E-08
3.06E-08	3.82E-08	3.76E-08	3.54E-08
3.80E-08	3.66E-08	3.09E-08	3.51E-08
3.59E-08	3.03E-08	3.64E-08	3.42E-08
3.12E-08	3.80E-08	3.79E-08	3.57E-08
3.76E-08	3.65E-08	3.00E-08	3.47E-08
3.68E-08	3.03E-08	3.68E-08	3.47E-08
3.07E-08	3.77E-08	3.75E-08	3.53E-08
3.82E-08	3.65E-08	3.03E-08	3.50E-08
3.63E-08	3.09E-08	3.59E-08	3.43E-08
3.09E-08	3.84E-08	3.79E-08	3.57E-08
3.86E-08	3.64E-08	2.97E-08	3.49E-08
3.62E-08	3.04E-08	3.68E-08	3.45E-08
3.15E-08	3.79E-08	3.75E-08	3.57E-08
3.77E-08	3.61E-08	3.06E-08	3.48E-08
3.59E-08	3.10E-08	3.74E-08	3.48E-08
3.23E-08	3.75E-08	3.79E-08	3.59E-08
3.79E-08	3.62E-08	3.05E-08	3.48E-08
			3.50E-08

Table 15: B field transmitted through core after 4 hours

4hours_1	4hours_2	4hours_3	avg
3.83E-08	3.53E-08	3.73E-08	3.70E-08
3.73E-08	3.44E-08	3.15E-08	3.44E-08
3.07E-08	3.87E-08	3.85E-08	3.60E-08
3.86E-08	3.31E-08	3.71E-08	3.62E-08
3.60E-08	3.52E-08	3.16E-08	3.43E-08
3.27E-08	3.84E-08	3.86E-08	3.66E-08
3.85E-08	3.26E-08	3.60E-08	3.57E-08
3.56E-08	3.63E-08	3.30E-08	3.50E-08
3.29E-08	3.84E-08	3.82E-08	3.65E-08
3.84E-08	3.22E-08	3.47E-08	3.51E-08
3.58E-08	3.71E-08	3.45E-08	3.58E-08
3.35E-08	3.85E-08	3.84E-08	3.68E-08
3.87E-08	3.17E-08	3.21E-08	3.42E-08
3.52E-08	3.66E-08	3.61E-08	3.60E-08
3.40E-08	3.88E-08	3.87E-08	3.72E-08
3.84E-08	3.09E-08	3.11E-08	3.35E-08
3.44E-08	3.72E-08	3.73E-08	3.63E-08
3.45E-08	3.84E-08	3.82E-08	3.70E-08
3.81E-08	3.01E-08	2.93E-08	3.25E-08
3.30E-08	3.77E-08	3.83E-08	3.63E-08
3.51E-08	3.83E-08	3.87E-08	3.74E-08
			3.57E-08

Table 16: B field transmitted through core after 6 hours

6hours_1	6hours_2	6hours_3	avg
3.76E-08	3.91E-08	4.01E-08	3.89E-08
3.25E-08	3.91E-08	4.00E-08	3.72E-08
3.95E-08	2.68E-08	4.00E-08	3.54E-08
3.66E-08	3.92E-08	4.02E-08	3.87E-08
3.34E-08	3.96E-08	3.97E-08	3.76E-08
3.97E-08	2.68E-08	4.04E-08	3.56E-08
3.70E-08	3.98E-08	3.98E-08	3.89E-08
3.38E-08	3.98E-08	4.01E-08	3.79E-08
4.01E-08	2.82E-08	3.98E-08	3.60E-08
3.57E-08	3.94E-08	3.98E-08	3.83E-08
3.52E-08	3.90E-08	3.99E-08	3.80E-08
3.96E-08	2.89E-08	4.03E-08	3.63E-08
3.48E-08	3.96E-08	4.01E-08	3.82E-08
3.54E-08	3.81E-08	3.99E-08	3.78E-08
3.97E-08	2.99E-08	4.02E-08	3.66E-08
3.34E-08	3.88E-08	4.02E-08	3.75E-08
3.69E-08	3.80E-08	3.98E-08	3.82E-08
3.94E-08	3.13E-08	4.00E-08	3.69E-08
3.28E-08	3.97E-08	3.99E-08	3.75E-08
3.75E-08	3.72E-08	4.05E-08	3.84E-08
3.96E-08	3.23E-08	3.94E-08	3.71E-08
			3.75E-08

Table 17: B field transmitted through core after 12 hours

12hours_1	12hours_2	12hours_3	avg
4.02E-08	3.97E-08	4.00E-08	4.00E-08
4.01E-08	4.07E-08	4.03E-08	4.03E-08
3.95E-08	3.97E-08	3.99E-08	3.97E-08
4.05E-08	4.04E-08	4.00E-08	4.03E-08
3.96E-08	3.95E-08	3.94E-08	3.95E-08
4.02E-08	4.00E-08	4.00E-08	4.01E-08
3.97E-08	3.96E-08	4.03E-08	3.99E-08
3.95E-08	3.96E-08	3.99E-08	3.97E-08
4.00E-08	4.03E-08	4.00E-08	4.01E-08
4.04E-08	4.01E-08	3.94E-08	4.00E-08
4.02E-08	3.97E-08	4.00E-08	3.99E-08
4.01E-08	4.01E-08	4.03E-08	4.02E-08
4.01E-08	4.02E-08	3.99E-08	4.01E-08
3.98E-08	3.99E-08	4.00E-08	3.99E-08
4.01E-08	4.02E-08	3.94E-08	3.99E-08
3.98E-08	4.00E-08	4.00E-08	4.00E-08
4.06E-08	4.05E-08	4.03E-08	4.05E-08
4.06E-08	3.99E-08	3.99E-08	4.01E-08
4.03E-08	4.00E-08	4.00E-08	4.01E-08
4.01E-08	3.95E-08	3.94E-08	3.97E-08
4.01E-08	4.02E-08	4.00E-08	4.01E-08
			4.00E-08

Table 18: B field transmitted through core after 18hours

18hours_1	18hours_2	18hours_3	avg
3.91E-08	3.84E-08	3.93E-08	3.89E-08
3.37E-08	3.87E-08	3.49E-08	3.58E-08
3.93E-08	3.58E-08	3.89E-08	3.80E-08
3.78E-08	3.88E-08	3.63E-08	3.76E-08
3.91E-08	3.54E-08	3.92E-08	3.79E-08
3.92E-08	3.91E-08	3.89E-08	3.91E-08
3.46E-08	3.91E-08	3.64E-08	3.67E-08
3.88E-08	3.67E-08	3.90E-08	3.82E-08
3.64E-08	3.98E-08	3.41E-08	3.68E-08
3.85E-08	3.38E-08	3.93E-08	3.72E-08
3.83E-08	3.88E-08	3.76E-08	3.82E-08
3.54E-08	3.89E-08	3.73E-08	3.72E-08
3.87E-08	3.80E-08	3.85E-08	3.84E-08
3.55E-08	3.93E-08	3.44E-08	3.64E-08
3.89E-08	3.36E-08	3.87E-08	3.71E-08
3.92E-08	3.86E-08	3.66E-08	3.81E-08
3.55E-08	3.76E-08	3.88E-08	3.73E-08
3.92E-08	3.95E-08	3.86E-08	3.91E-08
3.52E-08	3.99E-08	3.68E-08	3.73E-08
3.85E-08	3.57E-08	3.88E-08	3.77E-08
3.89E-08	3.89E-08	3.40E-08	3.73E-08
			3.76E-08

Table 19: B field transmitted through core after 24hours

24hours_1	24hours_2	24hours_3	avg
3.64E-08	3.60E-08	3.52E-08	3.59E-08
3.60E-08	3.43E-08	3.64E-08	3.56E-08
3.55E-08	3.63E-08	3.45E-08	3.55E-08
3.60E-08	3.55E-08	3.64E-08	3.60E-08
3.47E-08	3.60E-08	3.52E-08	3.53E-08
3.67E-08	3.61E-08	3.65E-08	3.64E-08
3.45E-08	3.62E-08	3.57E-08	3.55E-08
3.63E-08	3.61E-08	3.65E-08	3.63E-08
3.60E-08	3.55E-08	3.58E-08	3.58E-08
3.62E-08	3.64E-08	3.62E-08	3.63E-08
3.64E-08	3.51E-08	3.64E-08	3.60E-08
3.57E-08	3.64E-08	3.52E-08	3.57E-08
3.63E-08	3.44E-08	3.65E-08	3.57E-08
3.53E-08	3.68E-08	3.50E-08	3.57E-08
3.63E-08	3.49E-08	3.63E-08	3.58E-08
3.61E-08	3.63E-08	3.61E-08	3.62E-08
3.69E-08	3.69E-08	3.69E-08	3.69E-08
3.62E-08	3.60E-08	3.62E-08	3.61E-08
3.70E-08	3.63E-08	3.70E-08	3.68E-08
3.69E-08	3.69E-08	3.69E-08	3.69E-08
3.69E-08	3.69E-08	3.69E-08	3.69E-08
			3.61E-08

Table 20: B field transmitted through core after 36 hours

36hours_1	36hours_2	36hours_3	avg
3.55E-08	3.54E-08	3.68E-08	3.59E-08
3.70E-08	3.62E-08	3.54E-08	3.62E-08
3.55E-08	3.55E-08	3.67E-08	3.59E-08
3.68E-08	3.63E-08	3.41E-08	3.57E-08
3.52E-08	3.62E-08	3.68E-08	3.61E-08
3.68E-08	3.63E-08	3.36E-08	3.56E-08
3.64E-08	3.72E-08	3.64E-08	3.67E-08
3.63E-08	3.64E-08	3.40E-08	3.56E-08
3.67E-08	3.62E-08	3.65E-08	3.65E-08
3.60E-08	3.60E-08	3.45E-08	3.55E-08
3.59E-08	3.70E-08	3.67E-08	3.65E-08
3.67E-08	3.63E-08	3.52E-08	3.61E-08
3.67E-08	3.66E-08	3.63E-08	3.65E-08
3.60E-08	3.56E-08	3.60E-08	3.59E-08
3.60E-08	3.65E-08	3.63E-08	3.63E-08
3.57E-08	3.57E-08	3.61E-08	3.58E-08
3.62E-08	3.67E-08	3.69E-08	3.66E-08
3.56E-08	3.48E-08	3.62E-08	3.55E-08
3.64E-08	3.64E-08	3.70E-08	3.66E-08
3.62E-08	3.41E-08	3.69E-08	3.57E-08
3.64E-08	3.65E-08	3.69E-08	3.66E-08
			3.61E-08